# SYNTHESIS OF SILICA-BASED NANOMATERIALS AND THEIR APPLICATIONS IN FLUORESCENT, BIOLOGICAL AND CHEMICAL SENSING

A DISSERTATION SUBMITTED TO

THE GRADUATE SCHOOL OF ENGINEERING AND SCIENCE

OF BILKENT UNIVERSITY

IN PARTIAL FULFILLMENT OF THE REQUIREMENTS FOR

THE DEGREE OF

DOCTOR OF PHILOSOPHY

IN

MATERIALS SCIENCE AND NANOTECHNOLOGY

By

Pınar Beyazkılıç

June 2018

SYNTHESIS OF SILICA-BASED NANOMATERIALS AND THEIR APPLICATIONS IN FLUORESCENT, BIOLOGICAL AND CHEMICAL SENSING

By Pınar Beyazkılıç

June 2018

We certify that we have read this dissertation and that in our opinion it is fully adequate, in scope and in quality, as a dissertation for the degree of Doctor of Philosophy.

Çağlar Elbüken(Advisor)

Mehmet Bayındır(Co-Advisor)

Tarık Baytekin

Dönüş Tuncel

Uğur Tamer

Ersin Emre Ören

Approved for the Graduate School of Engineering and Science:

Ezhan Karaşan
Director of the Graduate School

# ABSTRACT

## SYNTHESIS OF SILICA-BASED NANOMATERIALS AND THEIR APPLICATIONS IN FLUORESCENT, BIOLOGICAL AND CHEMICAL SENSING

Pınar Beyazkılıç
Ph.D. in Materials Science and Nanotechnology
Advisor: Çağlar Elbüken
Co-Advisor: Mehmet Bayındır
June 2018

This thesis describes development of nanoparticle-based liquid sensors and coatings for droplet-based bioassays. Liquid sensors were produced from mesostructured (2-50 nm) hybrid silica nanoparticles. Detection of trace trinitrotoluene (TNT) and dopamine in aqueous phase was shown based on fluorescence of nanoparticles. Silica nanoparticles were synthesized using a facile one-pot sol-gel method. Pyrene molecules were hybridized with hydrophobic parts of cetyltrimethylammonium micelles followed by silica growth around micelles. Nanoparticles showed good dispersibility and colloidal stability in water. Pyrene exhibited bright and highly stable emission. Pyrene emission exhibited a rapid, sensitive and visual fluorescence quenching against TNT and dopamine.

For droplet-based assays, robust superhydrophilic patterned superhydrophobic coatings were developed. Biomolecular adsorption and droplet mixing were shown on coatings which were prepared using sol-gel method followed by ultraviolet/ozone (UV/O) treatment.

Droplet-based biomolecular detection platforms were developed using superhydrophilic patterned superhydrophobic surfaces. Benefitting from confinement and evaporation-induced shrinkage of droplets on wetted patterns, sensitive glucose and DNA detection was demonstrated. Glucose was detected based on enhancement of polydopamine (PDA) emission by hydrogen peroxide ($H_2O_2$) produced in glucose oxidation reaction. Detection in evaporating droplets resulted with bright fluorescence and high sensitivity for analyte molecules. This was due to droplet evaporation which concentrated molecules and increased reaction rates. Surfaces and nanoparticles developed in this thesis hold great potential for biological and chemical analysis with low sample volumes owing to their simple production, sensitive detection responses and versatility.

*Keywords:* silica nanoparticles, pyrene, superhydrophobic, superhydrophilic, glucose, DNA, dopamine.

# ÖZET

# SİLİKA NANOMALZEMELERİN SENTEZİ VE FLORESANS TABANLI BİYOLOJİK VE KİMYASAL SENSÖR UYGULAMALARI

Pınar Beyazkılıç
Malzeme Bilimi ve Nanoteknoloji, Doktora
Tez Danışmanı: Çağlar Elbüken
İkinci Tez Danışmanı: Mehmet Bayındır
Haziran 2018

Bu tez, nanoparçacık tabanlı geliştirilmiş sıvı sensörleri ve damlacık tabanlı biyosensörler için geliştirilmiş kaplamaları sunmaktadır. Sıvı sensörler mezoyapılı (2-50 nm) hibrit silika nanoparçacıklardan üretilmiştir. Nanoparçacıkların floresansı kullanılarak suda eser miktarda TNT ve dopaminin tespiti gösterilmiştir. Silika parçacıklar basit tek adımlı bir sol-jel yöntemi ile sentezlenmiştir. Pyren molekülleri, setiltrimetilamonyum misellerinin hidrokarbon zincirleriyle hibritleştirilmiştir ve sonra silika, misellerin etrafında büyütülmüştür. Nanoparçacıklar suda iyi dağılım ve koloidal kararlılık göstermiştir. Pyren, parlak ve oldukça kararlı floresans göstermiştir. Pyren floresansı, dopamin ve TNT' ye karşı; hızlı, hassas ve gözle görülebilir sönümlenme göstermiştir.

Damlacık tabanlı sensörler için, kalıcı süperhidrofilik (su seven) desenlere sahip süperhidrofobik (su sevmeyen) kaplamalar geliştirilmiştir. Sol-jel metodu ve ardından ultraviyole/ozon (UV/O) muamelesiyle hazırlanan kaplamalarla, biyomoleküler adsorpsiyon ve damlacık karıştırma gösterilmiştir.

Süperhidrofilik desenlere sahip süperhidrofobik yüzeylerle, damlacık tabanlı biyomolekül tespit platformları geliştirilmiştir. Damlacıkların, süperhidrofilik desenlerde sıkışması ve buharlaşmasına bağlı küçülmesinden yararlanarak hassas glukoz ve DNA tespiti gösterilmiştir. Glukoz, glukoz oksidasyonunda üretilen hidrojen peroksitin ($H_2O_2$) polidopamin (PDA) floresansını artırması temelinde tespit edilmiştir. Buharlaşan damlacıklarda yapılan tespit, analit moleküller için parlak floresans ve yüksek hassasiyetle sonuçlanmıştır. Bu, moleküllerin yüksek konsantrasyonlu olmasını ve reaksiyon hızlarının artmasını sağlayan damlacık buharlaşması sayesinde meydana gelmiştir. Bu tezde geliştirilen yüzeyler ve nanoparçacıklar; kolay üretimleri, hassas tespit cevapları ve kullanışlılıkları sayesinde düşük hacimli örneklerde biyolojik ve kimyasal analizler için büyük

potansiyele sahiptir.

*Anahtar sözcükler*: silika nanoparçacıklar, pyren, süperhidrofobik, süperhidrofilik, glukoz, DNA, dopamin.

# Acknowledgement

First and foremost, I would like to thank my advisor Prof. Çağlar Elbüken for his guidance and supports throughout my PhD. He always motivated me with my PhD and future career. The seven years in UNAM brought me great experience and extensive research skills. I owe my sincere thanks to Adem Yıldırım. He helped me for designing nanoparticles and sensing measurements. He also helped in writing manuscripts. I have learned a lot from him during these times.

Additionally, I would like to thank the professors in my thesis comittee; Dr. Mehmet Bayındır, Prof. Tarık Baytekin, Prof. Uğur Tamer, Prof. Ersin Emre Ören and Prof. Dönüş Tuncel. I wolud like to thank to professors who contributed to my thesis; Prof. Gökçen Demirel and Prof. Urartu Şeker. Without their comments and supports this thesis would be incomplete.

I would like to thank all present and past members of my research group and friends in UNAM. It will be a long list if I thank all of them one by one, but I would like to thank some of them particularly. To Abtin, my colleague, with him we failed and succeeded a lot. To Dilara for her valuable friendship. To my teammates and friends; Hülya, Abba, Arbab, Abubakar, Yunusa, Emre, Erol, Pelin, Ersin, Urandelger, Tahsin, Ziya, Murat, Ali, Elnaz, Muhammed; it was always fun to work with them. Also, I would like to thank all the staff and engineers of UNAM, especially Seda Kutkan, Gökçe Celik, Mustafa Güler, for their helps during measurements.

I would like to express my gratitude to The Scientific and Technological Research Council of Turkey (TÜBİTAK) BİDEB , for 2211 National Ph.D. Scholarship. This thesis was supported by TÜBİTAK under the project no. 111T696.

Last but not least, I would like to thank my family who always believed in me and supported me.

# Contents

# List of Figures

# Chapter 1

# Introduction

A sensor detects physiological changes or chemical and biochemical information by its receptor element and converts into an analytical signal and transmits to a detector [1]. Analytical signal produced by a sensor can be electrochemical, optical, acoustic, piezoelectrical or thermal. A biosensor transducer contains a biological element such as enzyme, antibody or DNA as receptor which specifically binds to analyte species including glucose, DNA or antigen. Biosensors are classified based on their transducer type; enzymatic, immunoaffinity, whole-cell, aptamer and DNA [2].

Biosensors have been a significant research area in analytical chemistry since they have been applied in various fiels such as medical diagnosis, environmental safety and military. An ideal biosensor must generate accurate, fast and sensitive results [3]. Towards ideal sensor production, numerous new systems and materials have been introduced over the past few decades. Nanomaterials have attracted huge interest in biological and chemical sensing owing to their high surface-to-volume ratio; tunable size and shape as well as unique chemical, thermal and electrical properties. For example, carbon nanotubes with superior electrical properties have been used in modern electrochemical biosensors and revealed high sensitivity and selectivity [4]. Although electrochemical detection occupies the majority of transduction in sensors, optical methods have been also

widely used. Optical methods include fluorescence and absorption spectrophotometry, raman spectroscopy, refractive index and light scattering. Nanomaterials have constituted important application in optical sensors due to the unique radiative properties arised from small sizes [5]. Nanoparticles made from noble metals such as gold and silver have introduced a very sensitive way for molecular detection based on raman spectroscopy called surface enhanced raman spectroscopy (SERS). Among the optical sensors, fluorescence has been very widely used since it can be applied to a variety of materials and it is sensitive. Fluorescence detection involves an indicator with intrinsic fluorescence radiation which is then changed as a response to the presence of an analyte. Typically fluorescent indicator or 'probe' is encapsulated to a support matrix which can be metal, polymer or ceramic [6, 7]. Numerous new classes of fluorescent nanomaterials have been developed towards chemical and biomedical sensing such as silica, polymers, semiconductors and proteins [8]. Fluorescent nanomaterials have also been used for bioimaging and labeling in cells and disease theraphy [9]. Among them, silica-based nanomaterials have been very promising owing to their tunable size and shape, high porosity, good molecule hosting properties, good photophysical characteristics and surface tailorability.

In this thesis, silica nanomaterials were designed and synthesized for sensitive detection of toxic material and biological molecules. Sensor materials have been prepared in the form of colloidal aqueous solutions or in the form of porous thin films.

This thesis is organized in seven chapters. In Chapter 1, general information about sensors and motivation of the thesis are stated.

In Chapter 2, synthesis of organic-inorganic hybrid mesoporous silica nanoparticles is reported. Silica nanoparticles were doped with a hydrophobic fluorescent dye called pyrene. As-synthesized nanoparticles were used for trinitrotoluene (TNT) detection in aqueous solutions.

In Chapter 3, application of hybrid nanoparticles towards dopamine detection is reported. Dopamine is a neurotransmitter found in biological fluids. Pyrene

was uniformly dispersed in water by encapsulating in mesostructures of silica nanoparticles without any chemical modification and used as a fluorescent probe for dopamine.

In Chapter 4, preparation of organically modified silica (ormosil) thin films with highly porous and superhydrophobic characteristics is described. Ormosil coatings were produced using a one-pot sol-gel method. Then, superhydrophilic patterns were generated on selected areas of superhydrophobic coatings using a simple mask-aided UV/Ozone treatment method. Potential use of patterned surfaces in high-throughput biological assays and microarray applications is demonstrated.

In Chapter 5, fluorescence-based glucose detection using polydopamine (PDA) and superhydrophilic-patterned surfaces is shown. PDA emission during its in situ formation from dopamine was turned on in the presence of glucose and glucose oxidase enzyme due to oxidation by $H_2O_2$ which is enzymatically produced. $H_2O_2$-dependent fluorescence enhancement of PDA was combined with superhydrophilic/superhydrophobic patterned surfaces and a sensitive droplet-based glucose sensing strategy was developed.

In Chapter 6, functionalization of wetted patterns with epoxy groups and nucleotide sequences and their application for droplet-based DNA sensing are presented.

In Chapter 7; concluding remarks are stated.

# Chapter 2

# Mesostructured Silica Nanoparticles for Aqueous Phase Trinitrotoluene (TNT) Detection

Detection of trinitrotoluene (TNT) in water is of great importance since it contaminates water resources and is highly toxic to the biological organisms [10,11]. Currently, ion mobility spectroscopy (IMS) and mass spectrometry are used for TNT detection [12–15]. Besides to such sensitive methods, development of simple and handheld techniques such as fluorescence based systems (consisting of a simple UV lamp and a fluorescent probe) have been important owing to their portability properties. Quantum dots and fluorescent dyes can detect TNT in aqueous phase [16–27]. However, these methods generally have laborious and costly synthesis. Therefore, there is still need for sensors with good sensitivity and easy production.

In this thesis, pyrene confined mesostructured silica nanoparticles (pMSNs) were developed for TNT detection in water. Fluorescence of pyrene which is a polycyclic fluorophore is quenched by TNT through photoinduced electron transfer (PET) [28, 29]. Excimer emission of pyrene observed in the presence of $\pi$-$\pi^*$

stacking interaction between excited and ground state pyrene molecules, is sensitive for TNT. Recently, pyrene excimer fluorescence was used towards TNT detection with nanomaterials that hybridized with chemically or physically attached pyrene [30–37]. However, most of such materials detected TNT in gas phase and in organic solvents [31–34].

This thesis demonstrates trace level (nM) detection of TNT in aqueous solutions using pMSNs. In order to confine pyrene molecules in nanoparticles, hydrophobic pyrene molecules were hybridized with hydrophobic parts of rod-shaped cetyltrimethylammonium (CTA) micelles. Silica was grown around micelles using tetraethyl orthosilicate (TEOS) and pyrene/silica organic/inorganic hybrid nanoparticles were obtained. Similar surfactant-assisted methods to load water-soluble dyes (e. g. R6G) into pores of mesostructured silica nanoparticles (MSNs) have been reported [38, 39]. In this study, surfactant assisted loading of a water-insoluble molecule into pores of MSNs is shown. Excimer emission of pyrene confined in mesostructured nanoparticles was bright. Furthermore, excimer emission was stable for at least six months. Benefitting from such stability, TNT detection performance of nanoparticles in water was investigated relying on on excimer emission quenching.

## 2.1 Experimental Section

### 2.1.1 Materials

Tetraethyl orthosilicate (TEOS), chloroform, and sodium hydroxide were purchased from Merck. Pluronic® F127, cetyltrimethylammoniumbromide (CTAB) and pyrene were purchased from Sigma-Aldrich. All chemicals were used as received without any purification. Deionized (DI) water (18.2 MΩ.cm at 25 °C) was obtained using a Millipore Milli-Q water purification system (Billerica).

### 2.1.2 Synthesis of pyrene confined mesostructured silica nanoparticles

Pyrene confined mesostructured silica nanoparticles (pMSNs) were synthesized by slightly modifying the common MCM-41 type MSN synthesis methods [40–43]. 6, 12, 22 or 40 mg of pyrene was dissolved in 500 $\mu$L of chloroform which was mixed with 30 mL of aqueous solution containing 200 mg of CTAB. Mixture was stirred at 60 °C for 20 min. For silica growth reaction, 20 mg of F127 and 66 mL of deionized water and 0.7 mL of 2.0 M sodium hydroxide solution was mixed. Then, CTAB solution was added and heated to 80 °C. Then, 1 mL of TEOS was added. Reaction mixture was stirred at 600 rpm for 2 h. When finished, particles were purified with three cycles of centrifugation (at 9000 rpm) and rinsing with deionized water.

### 2.1.3 Fluorescence quenching experiments

Fluorescence quenching experiments were performed in quartz cuvettes. 3 mL of pMSNs dispersions were used for each concentration. Fluorescence spectrum of pMSNs dispersions were recorded before and after addition TNT aqueous solutions with concentrations ranging from 10 nM to 10 $\mu$M (excitation wavelength used was 340 nm). Fluorescence quenching analysis was performed using 10.0 $\mu$M aqueous solutions of trinitrotoluene, dinitrotoluene, nitrobenzene, benzoic acid, aniline, chloroform, methanol, hydrochloric acid, sodium hydroxide and sodium chloride.

### 2.1.4 Characterization

Structure of pMSNs was investigated with transmission electron microscope (TEM, Tecnai G2-F30, FEI) and scanning electron microscope (SEM, Quanta 200F, FEI). Absorption spectrum of pMSNs was recorded with UV-Visible spectrophotometer (Cary 100, Varian). Fluorescence spectra of pMSNs were recorded

with fluorescence spectrophotometer (Cary Eclipse, Varian). Visual TNT detection experiments were performed using a UV inspection cabinet (Camag) with a light source operating at 366 nm. Size distribution and zeta potential of nanoparticles were analysed using a zetasizer (Malvern Instruments).

## 2.2 Results and Discussion

Pyrene confined mesostructured silica nanoparticles (pMSNs) were produced for trace detection of trinitrotoluene (TNT) in aqueous phase. pMSNs were synthesized upon TEOS polymerization around CTAB surfactant micelles in basic sodium hydroxide solution. Basic solution was used for efficient self-assembly of negatively charged silicates with positively charged cetyltrimethylammonium (CTA) micelles [44]. Pyrene was hybridized with hydrophobic parts of the CTA micelles and added to silica growth reaction mixture (Figure 2.1). CTA micelles both templated for meso (2-3 nm) pores and acted as nanocontainer for pyrene. Pluronic® F127, a nonionic surfactant was used to prevent particle aggregation enhance colloidal stability of nanoparticles (Figure 2.1) [45].

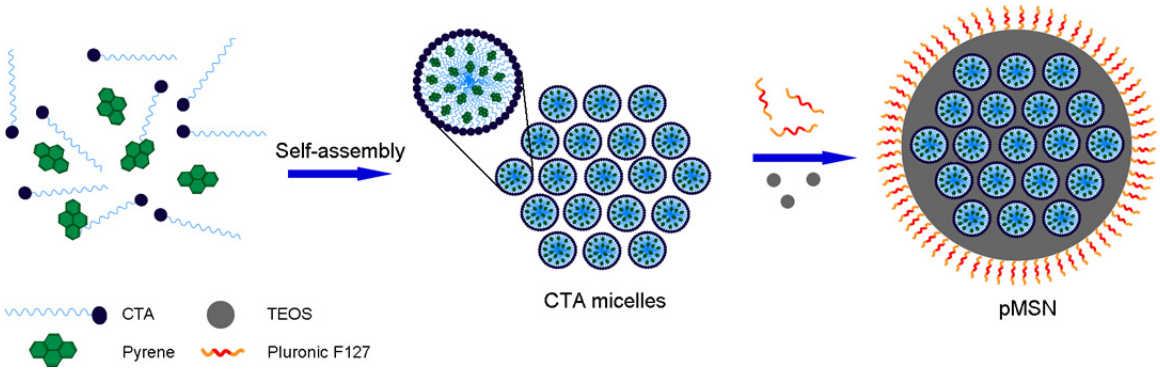


Figure 2.1: Schematic representation for formation of pyrene/mesostructured silica nanoparticles (pMSNs) hybrids.

Figure 2.2 shows TEM and SEM images of pMSNs prepared using 40 mg of pyrene. pMSNs have mesostructures with sizes around 2-3 nm. pMSNs were

sphere-shaped with average particle size of 74∓9 nm. In addition, pMSNs were analyzed synthesized using 6, 12, and 22 mg of pyrene. Effect of pyrene concentration on size and shape of nanoparticles was significant. 6 and 22 mg of pyrene resulted with rod-like shaped particles and polydispersity (Figure 2.3).

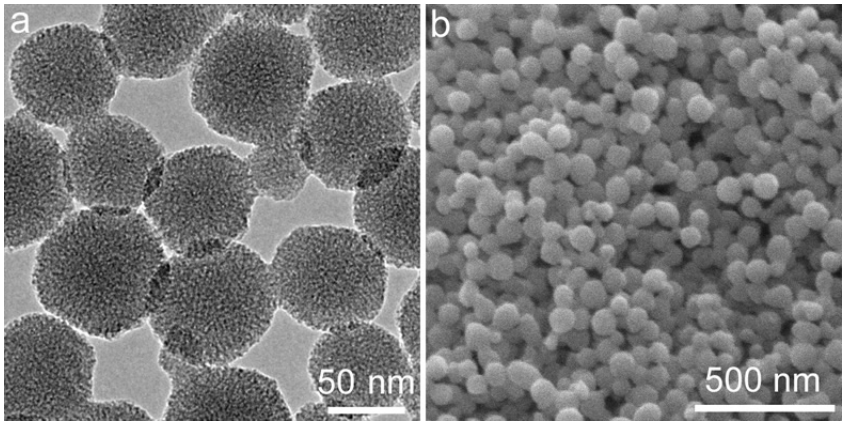


Figure 2.2: (a) TEM, and (b) SEM images of the pMSNs prepared using 40 mg of pyrene.

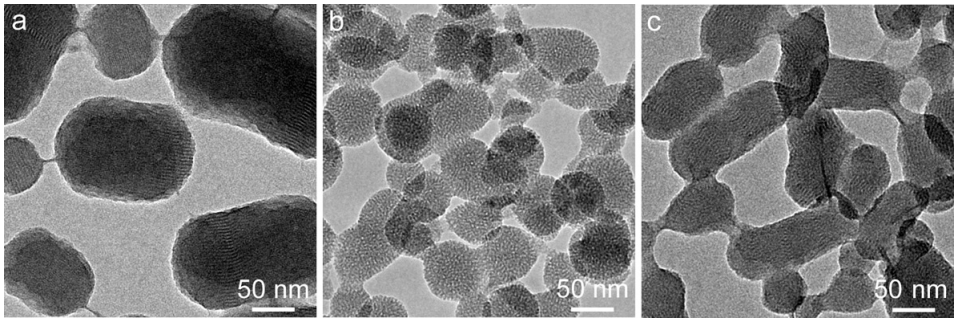


Figure 2.3: TEM images of pMSNs prepared using (a) 6 mg, (b) 12 mg, and (c) 22 mg of pyrene.

Figure 2.4 shows UV-visible absorption spectrum and fluorescence spectrum of pMSNs. Peaks at 304, 321, and 336 nm in the absorption spectrum are characteristic absorption bands of pyrene [46]. Emission bands around 370-400 nm in the fluorescence spectrum correspond to monomer emission which occurs upon radiative relaxation of excited electron in single pyrene [46]. Broad emission peak centered at 475 nm is excimer emission which is formed upon excitation of

two pyrene molecules in $\pi$-$\pi^*$ stacking interaction [47]. pMSNs prepared using 40 mg of pyrene were used in all performance measurements owing to their more uniformly distributed particle size.

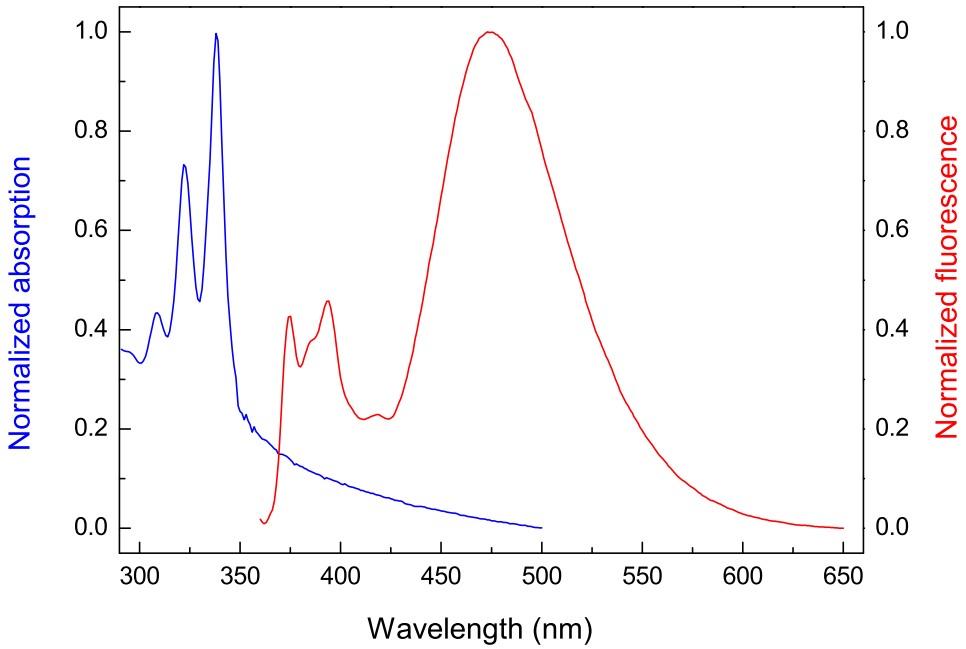


Figure 2.4: UV-Visible absorption spectrum (blue) and fluorescence emission spectrum (red) of pMSNs. Excitation wavelength was 340 nm). Three peaks observed at 304, 321, and 336 nm are absorption bands of pyrene. Peaks at 370-400 nm are monomer emission while band centered at 475 nm is excimer emission.

Leakage of pyrene from nanoparticles decreases excimer emission. In order to check encapsulation stability of pyrene, pMSNs dispersion was centrifuged and supernatant emission was measured. Supernatant had no emission indicating stable pyrene hybridization in nanoparticles (Figure 2.5).

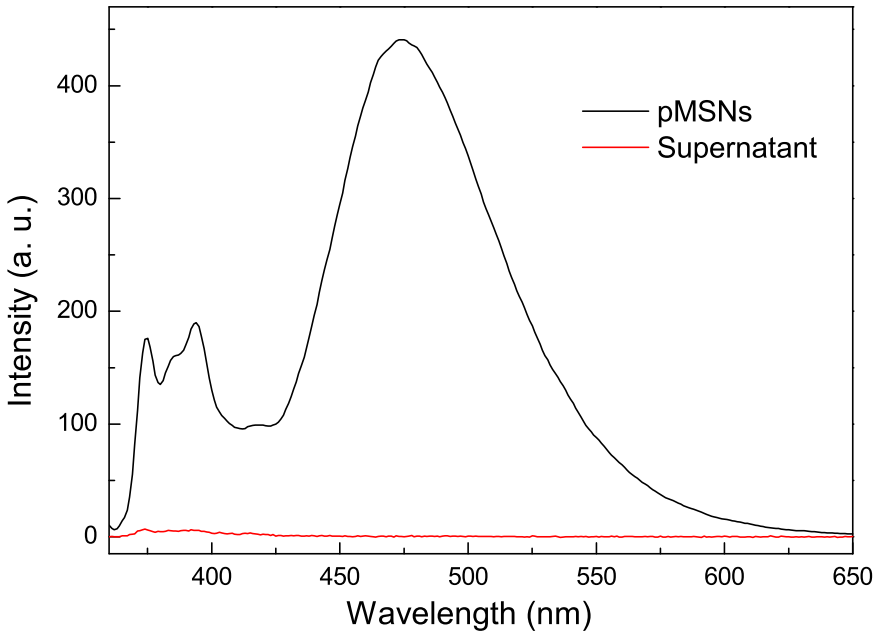


Figure 2.5: Fluorescence spectra of pMSNs (black) and supernatant (red) of pMSNs which was obtained after centrifugation.

After six-month-storage, pMSNs emission was bright close to that in as-prepared particles (Figure 2.6).

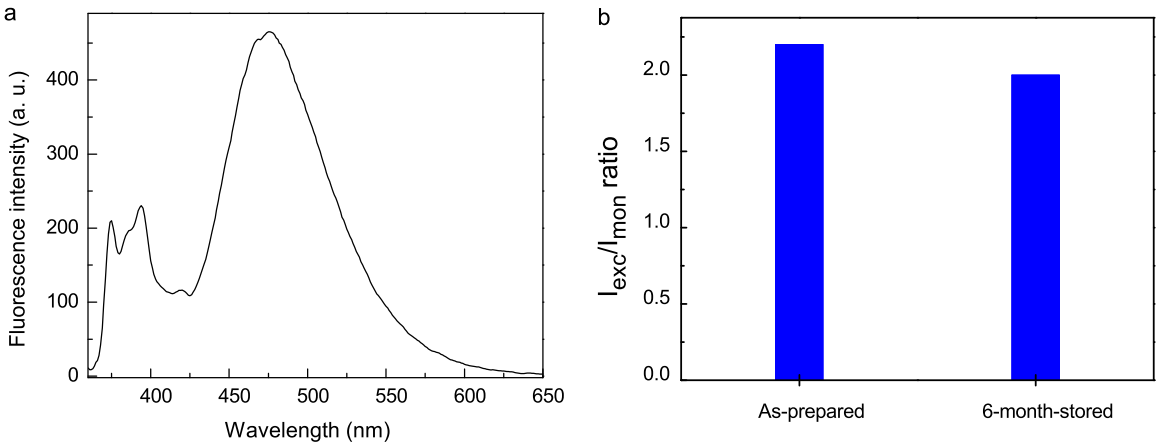


Figure 2.6: Fluorescence spectrum of pMSNs which was stored for six months at ambient conditions.

Size distribution of pMSNs was measured using dynamic light scattering (DLS) technique. Average particle size was measured as 84.8 nm (Figure 2.7a), which was very close to value calculated from TEM images, revealing good dispersibility in water. Furthermore, zeta potential of nanoparticles was measured to determine surface charge. Nanoparticles was positively charged with a potential of 33.8 mV due to positively charged CTA micelles. To investigate colloidal stability, pMSNs were analyzed with DLS time-dependently. Average particle size remained stable revealing that particle do not aggregate during measurements (Figure 2.7b).

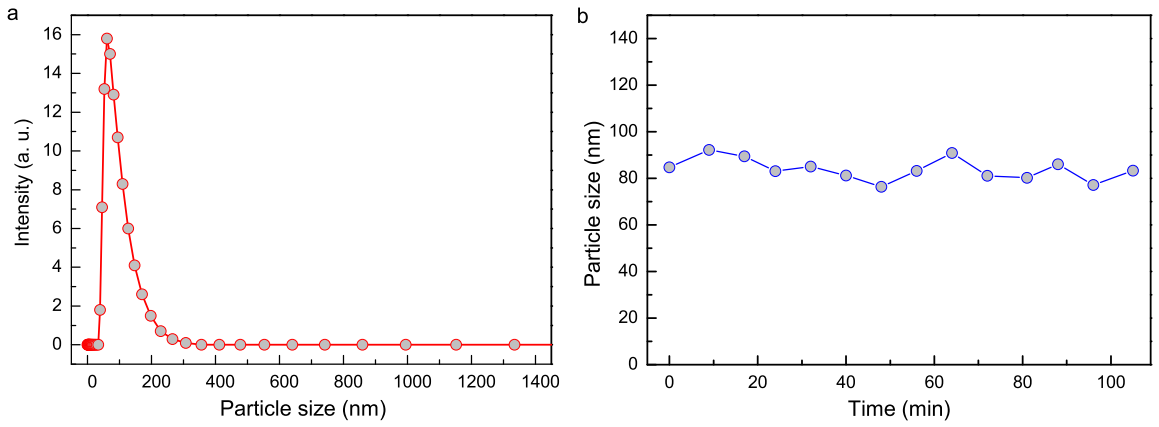


Figure 2.7: a) Particle size distribution of pMSNs measured using dynamic light scattering technique. b) Average particle size of pMSNs with respect to time.

Binding of TNT to pyrene through $\pi$-$\pi^*$ interaction resulted with quenching of strong excimer emission through photoinduced electron transfer (PET) from excited pyrene excimers to TNT [29]. Both monomer and excimer emission intensities were quenched with increasing TNT concentration ranging from 10 nM to 10 $\mu$M (Figure 2.8).

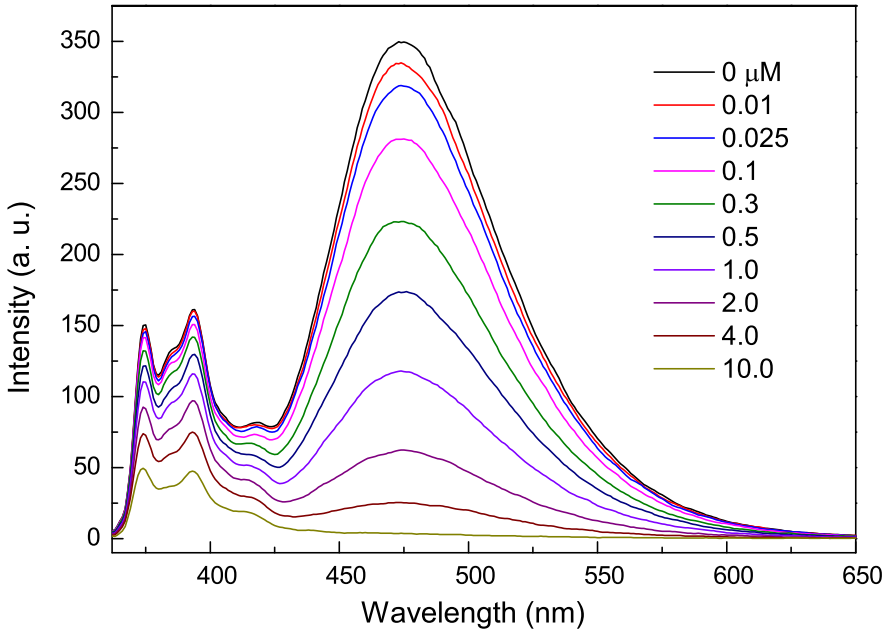


Figure 2.8: Fluorescence emission spectra of pMSNs with increasing TNT concentration ranging from 10 nM to 10 $\mu$M.

Figure 2.9 shows rate of signal stabilization. Emission stabilized within 45 s after addition of TNT and remained constant up to five min. When TNT was absent, excimer emission was constant.

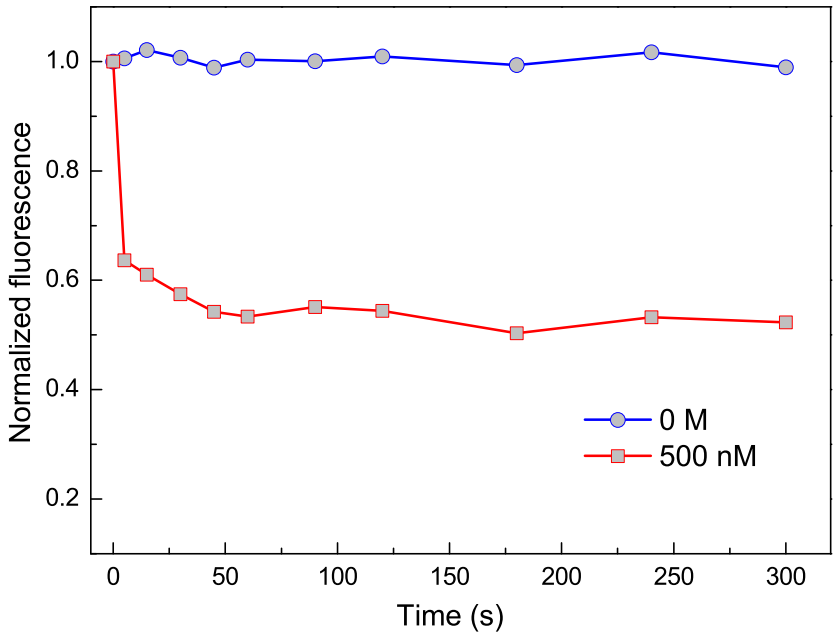


Figure 2.9: Time-dependent excimer emission intensity of pMSNs in the absence and presence of 500 nM TNT.

Figure 2.10 shows quenching efficiencies in excimer and monomer emission depending on TNT concentration. Quenching efficiency in excimer emission was 3.1% for 10 nM TNT and reached to 67.2% when 1.0 $\mu$M TNT was added. On the other hand, quenching efficiency in monomer emission was lower than that in excimer emission which shows higher sensitivity of excimer emission towards TNT. Limit of detection was calculated to be 12 nM using fitted linear curve showing quenching efficiency against concentration (Figure 2.11).

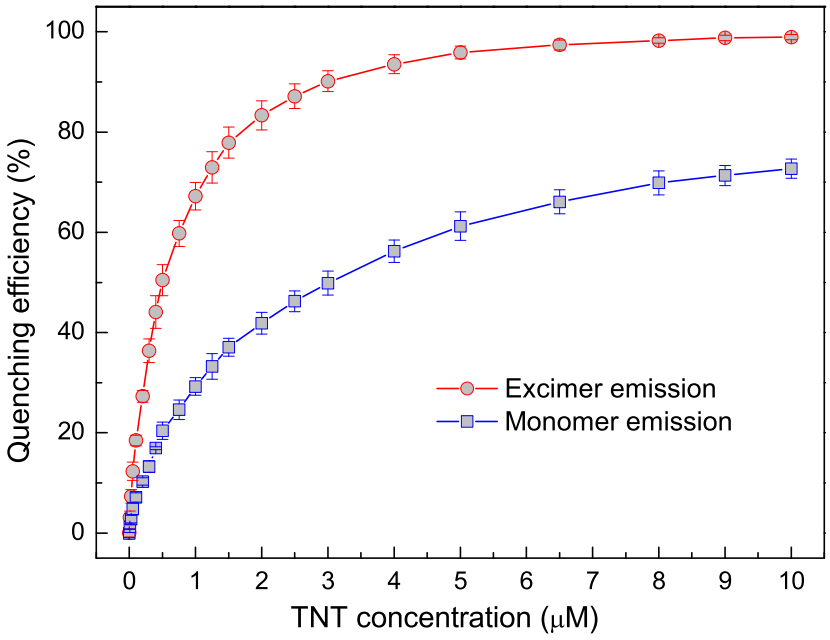


Figure 2.10: Quenching efficiencies of pMSNs depending on TNT concentration based on excimer emission (at 475 nm) and monomer emission (at 394 nm). Intensities are averages of three repeated measurements. Error bars show standard deviation.

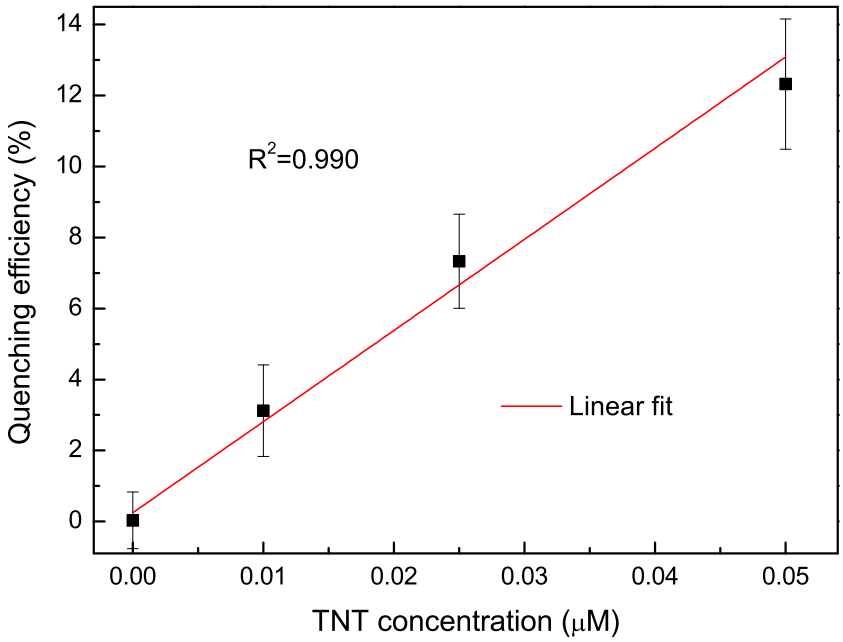


Figure 2.11: Linear fitted curve for quenching efficiency against concentration range from 0.01 to 0.05 $\mu$M TNT based on excimer emission (at 475 nm). Linear curve with the highest regression coefficient ($R^2$=0.99) was plotted with the lowest four concentration values.

Besides higher quenching efficiency in excimer emission, bright blue colour of excimer emission enabled colorimetric TNT detection. Accordingly, fluorescence of nanoparticles in the presence of 0.4 $\mu$M, 1.0 $\mu$M, 4.0 $\mu$M, and 8.0 $\mu$M TNT was measured under UV light (366 nm) illumination (Figure 2.12). Upon addition of 0.4 $\mu$M TNT, which was found to quench emission by 44.1% based on spectroscopy, color weakening was clearly observed under UV light. No color was observed upon addition of 8.0 $\mu$M TNT.

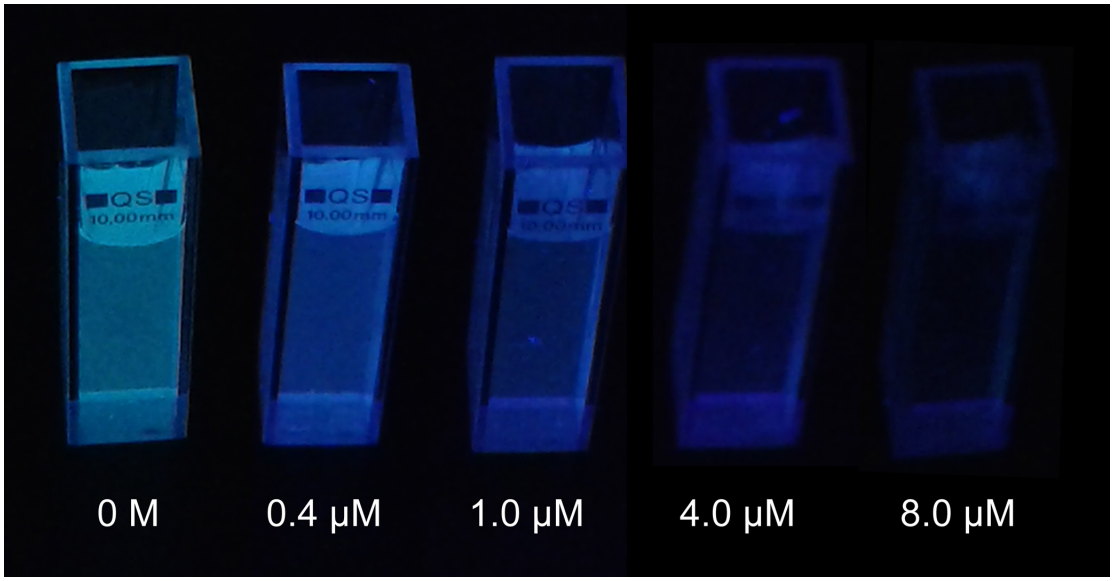


Figure 2.12: Optical photographs of pMSNs dispersions under UV-light before and after the addition of 0.4 $\mu$M, 1.0 $\mu$M, 4.0 $\mu$M, and 8.0 $\mu$M of TNT.

Fluorescence quenching of pMSNs against 10.0 $\mu$M TNT-similar and various other substances was measured. Figure 2.13 shows quenching efficiencies in excimer emission after testing analytes. Quenching efficiency for TNT was 98.9% whereas it was 40.0% and 25.0% for dinitrotoluene (DNT) and nitrobenzene (NB), respectively. On contrary to this; chloroform, sodium hydroxide, benzoic acid, aniline, sodium chloride, methanol and hydrochloric acid did not quenched emission significantly. High quenching efficiencies for DNT and NB compared to that for other analytes were due to their similar molecular structure to TNT [15, 48].

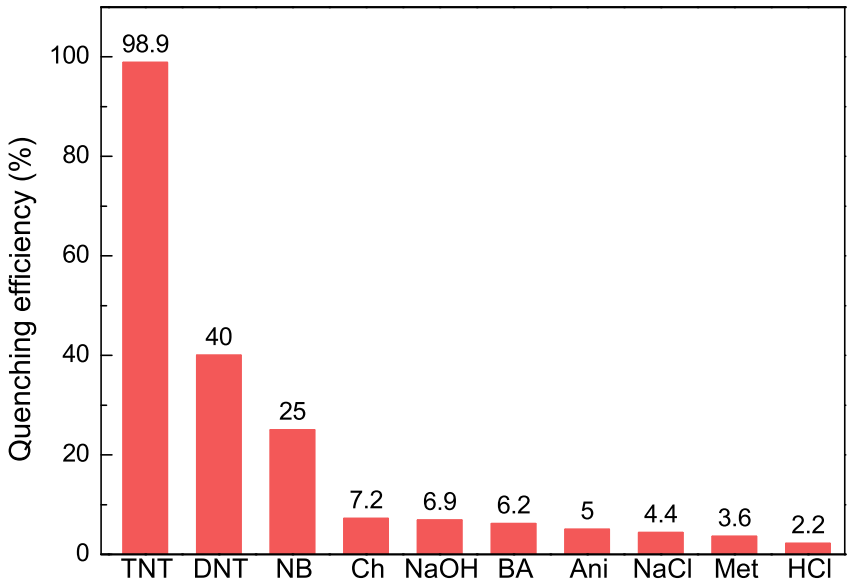


Figure 2.13: Fluorescence quenching efficiencies of excimer emission for10.0 $\mu$M aqueous solutions of various analytes (TNT: trinitrotoluene, DNT: dinitrotoluene, NB: nitrobenzene, Ch: chloroform, NaOH: sodium hydroxide, BA: benzoic acid, Ani: aniline, NaCl: sodium chloride, Met: methanol, and HCl: hydrochloric acid).

Since portable and simple platforms are desired for on-site TNT analysis, pMSNs were adapted to a microfluidic chip designed with valves that can be turned on and off. The microfluidic device was made of polydimethylsiloxane (PDMS); included a serpentine test channel, a straight control channel (300 $\mu$m width, 100 $\mu$m height) and two reservoirs (6 mm x 2 mm) for qualitative observation (Figure 2.14a). Plug microvalves were placed after the reservoirs to control the flow along the control and test channels. Flow is generated by applying negative pressure at the shared outlet using a 0.5 ml syringe. Solution of pMSNs was introduced to inlet 1 and TNT solution (0.25 mM) was introduced to inlet 2. After applying vacuum, the valves were turned ON sequentially. In the serpentine test channel,

TNT solution was mixed with pMSNs and filled the test reservoir whereas unmixed pMSNs followed the straight channel and filled the control reservoir. Then, the reservoirs were imaged under UV illumination (366 nm) for fluorescent detection.The control reservoir showed a bright blue color while the test reservoir was pale blue since fluorescence of pMSNs was quenched by TNT molecules (Figure 2.14b). As a control experiment, pMSNs were mixed instead of water by following the same procedure. Mixing with water indicated no influence of dilution on fluorescence signal as shown in Figure 2.14b. Whole mixing and analysis time was two minutes. This simple device demonstrates the potential of pMSNs to be used in portable microfluidic detection devices.

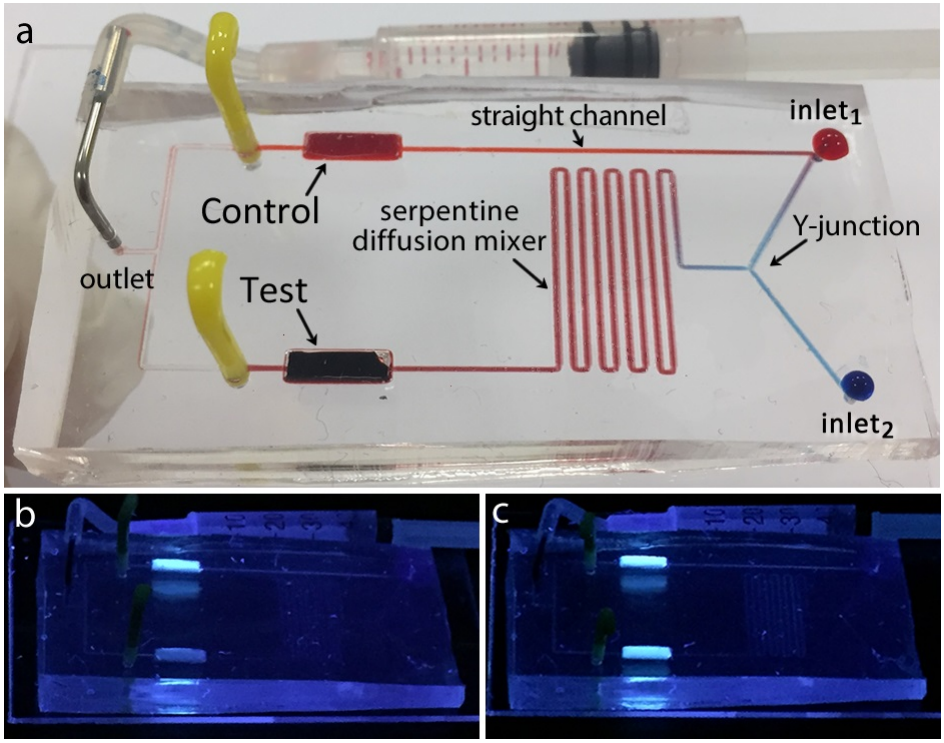


Figure 2.14: (a) Plug microvalve-integrated device for rapid and portable qualitative TNT detection. Fluorescent silica nanoparticle and TNT solution were introduced at two inlets. Mixing of TNT and nanoparticle solutions lead to fluorescence quenching in the test channnel. (b) Device tested with TNT solution under UV light (366 nm) excitation. (c) Control assay run with water instead of TNT solution.

In conclusion, a facile and low-cost method was developed to prepare pyrene confined mesostructured (pMSNs) silica nanoparticles for sensitive detection of TNT in water. Pyrene was encapsulated in mesostructured nanoparticles through hydrophobic-hydrophobic interactions between CTA micelles and pyrene. Spherical hybrid nanoparticles showed good colloidal stability in water. Bright excimer emission of pMSNs exhibited rapid quenching against TNT.

# Chapter 3

# Hybrid Silica Nanoparticles for Fluorescence-Based Detection of Dopamine

Dopamine (DA) is a neurotransmitter which has many important brain and cardiovascular functions [49, 50]. Since dysfunction of DA may be an indication of diseases such as Parkinson and Alzheimer, its diagnosis is crucial [51]. Electrochemical methods have been commonly used towards detection of DA [52]. However, they have some limitations such as interference from uric acid and ascorbic acid. Fluorescent probes with their high sensitivity have attracted great interest for DA detection. Several sensors have been developed towards DA detection based on fluorescent quenching using quantum dots, graphene oxide and gold nanoparticles [53, 54]. However, synthesis of fluorescent probes for DA detection involves complicated and time-consuming procedures.

In this thesis, a simple fluorescent DA sensor was developed using pyrene hybridized mesostructured silica nanoparticles (pMSNs). pMSNs were synthesized by following the procedure explained in Chapter 2. Since rod-shaped nanoparticles were used, rod-shaped nanoparticles were abbreviated as r-pMSNs in this chapter.

## 3.1 Experimental Section

### 3.1.1 Synthesis of pyrene confined mesostructured silica nanoparticles

Rod-shaped silica nanoparticles were synthesized using 21 mg of pyrene and characterized as described in Chapter 2.

### 3.1.2 Fluorescence quenching experiments

Fluorescence quenching experiments were performed in quartz cuvettes. First, 10 mM tris buffer solution was prepared and its pH was adjusted to 8.6 using 2 M hydrochloric acid. 0.020 mg/mL r-pMSNs in 3 mL of tris buffer solutions were used for each sensing measurement. Fluorescence spectrum of nanoparticle dispersions were recorded before dopamine addition (excitation wavelength was 340 nm). Then, dopamine aqueous solutions were added in order to adjust dopamine concentrations ranging from 0.5 $\mu$M to 30 $\mu$M. Fluorescence intensities were measured after 30 min. Fluorescence quenching of nanoparticles was investigated using 100 $\mu$M aqueous solutions of sucrose, ascorbic acid, sodium ion, potassium, calcium ion, chloride ion, lysine, alanine, aspartic acid, uric acid and glucose.

## 3.2 Results and Discussion

Fluorescence quenching of r-pMSNs depending on dopamine (DA) concentration was exploited for dopamine detection. Figure 3.1 shows transmission electron microscopy (TEM) and scanning electron microscopy (SEM) images of r-pMSNs. Addition of 21 mg of pyrene led to the formation of r-pMSNs with uniform morphology. Nanorods had a thickness around 65 nm and an aspect ratio ranging

from 2 to 5.5.

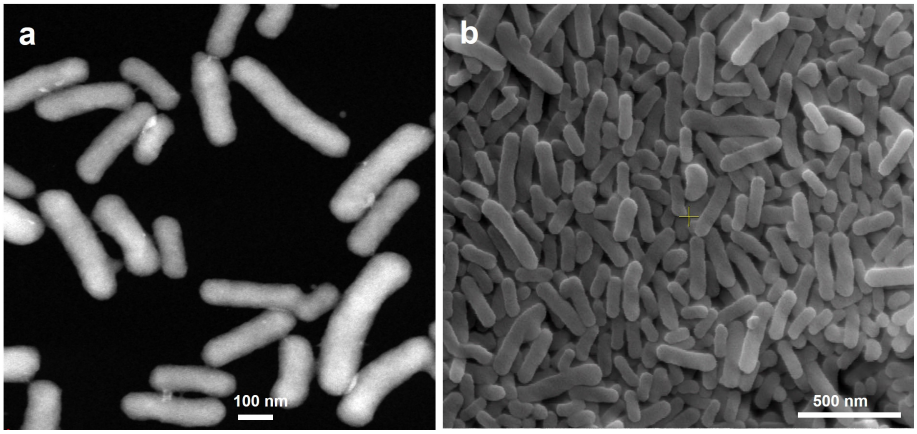


Figure 3.1: a) TEM and b) SEM images of the rod-shape pyrene confined mesostructured silica nanoparticles (r-pMSN).

In tris-buffer solution (pH= 8.6), DA oxidizes to quinone which acts as electron acceptor due to its electron deficiency (Figure 3.2). To evaluate sensing performance, nanorods were dispersed in 3 mL tris-buffer solutions since DA is oxidized under basic conditions. Fluorescence of r-pMSNs was measured and DA was added. Figure 3.3 shows fluorescence spectra recorded after incubation with DA for various concentrations. Bands at 370-394 nm and 475 nm which are characteristic monomer and excimer emission of pyrene, respectively, were both quenched gradually with increasing DA concentration.

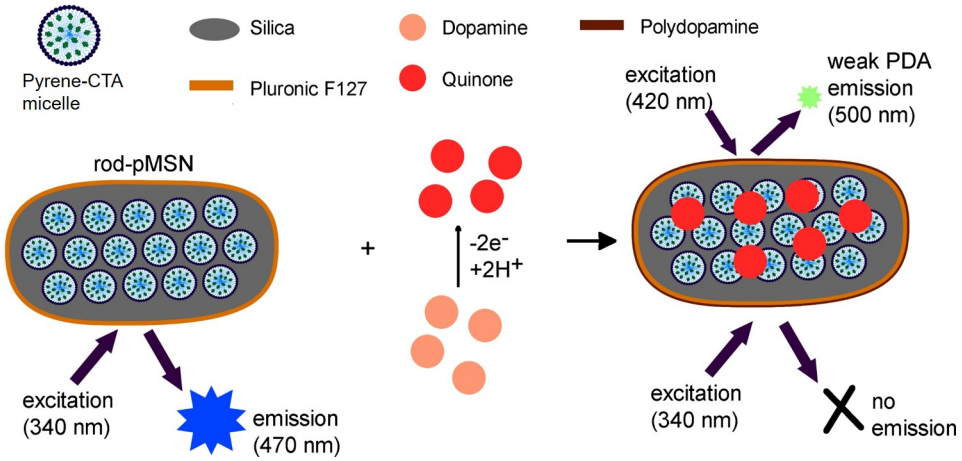


Figure 3.2: Electron transfer from rod-shape hybrid silica nanoparticles to quinone; oxidized dopamine (DA) and DA detection based on electron transfer induced fluorescent quenching.

Figure 3.3b shows quenching efficiencies with respect to DA concentration ranging from 1 $\mu$M to 30 $\mu$M. Quenching efficiency linearly increased from 1 $\mu$M to around 15 $\mu$M and slightly increased with 25 $\mu$M (Figure 3.3b and Figure 3.4). Limit of detection was calculated to be around 300 nM using linear curve fitted from 1 $\mu$M to 15 $\mu$M.

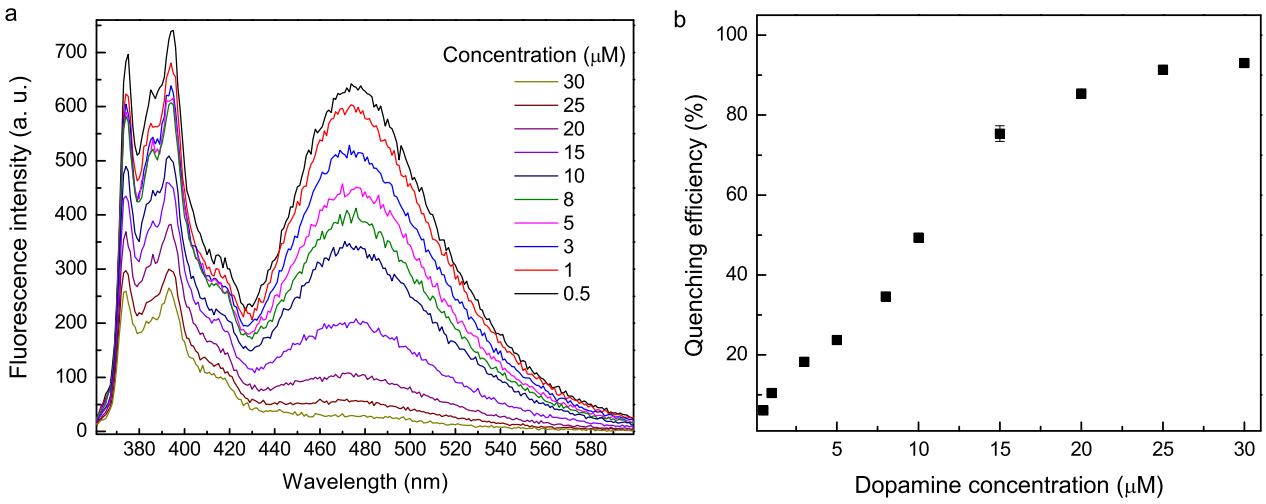


Figure 3.3: a) Fluorescence spectra of r-pMSNs sensor assay as a function of DA concentration ranging from 0.5 to 30 $\mu$M. Excitation wavelength used was 340 nm. b) Quenching efficiencies of the r-pMSNs sensor assay calculated as a function of DA concentration ranging from 0.5 to 30 $\mu$M .Intensities are averages of three repeated measurements. Error bars show standard deviation.

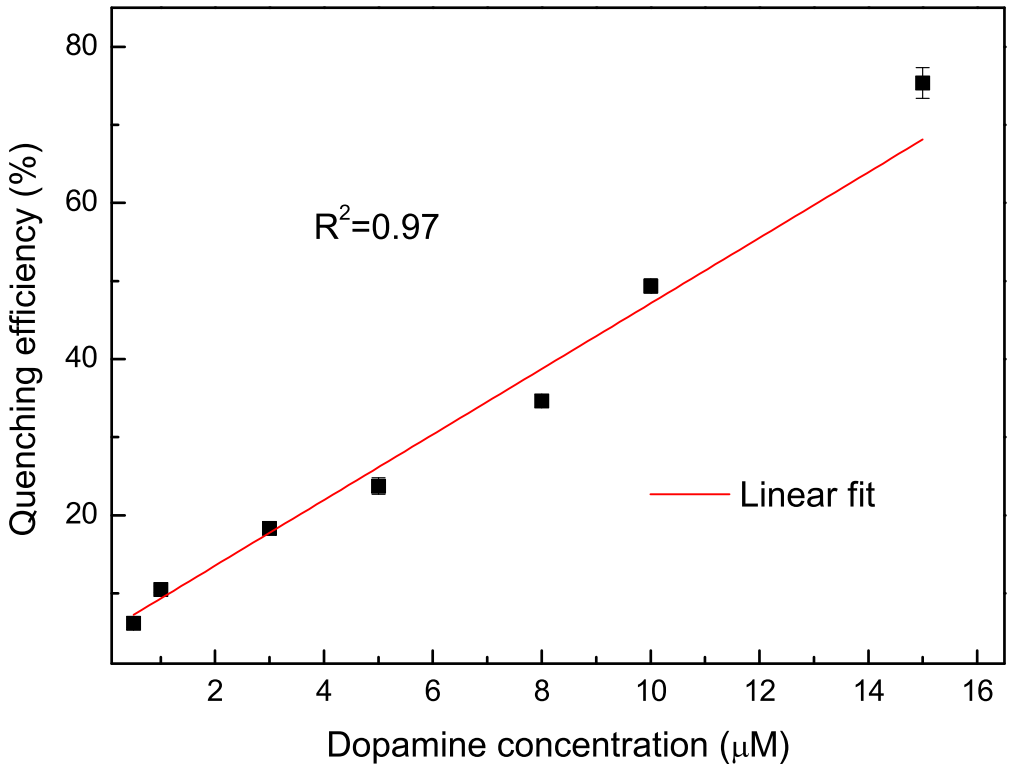


Figure 3.4: Linear fit of quenching efficiencies in the range from 0.5 to 15 $\mu$M dopamine concentration. Linear curve with the highest regression coefficient ($R^2$=0.97) was plotted with the lowest eight concentration values.

Furthermore, colorimetric dopamine detection was demonstrated by exploiting the bright blue excimer emission of pyrene which can be observed under UV excitation. Figure 3.5 shows colorimetric assay illuminated under UV light (366 nm). While fluorescence of r-pMSNs was very bright in the absence of DA. Color intensity reduced upon incubation with 3 $\mu$M DA. Gradual color weakening with increasing DA concentration can be clearly realized. Then, emission was significantly quenched upon addition of 10 $\mu$M TNT.

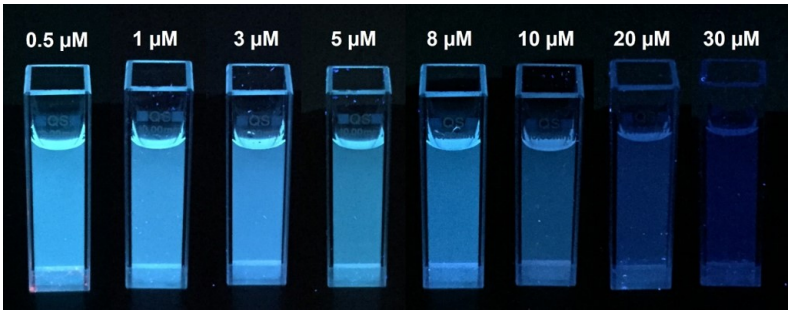


Figure 3.5: Visual detection capability of r-pMSNs assay. Assays after incubated with DA with concentration ranging from 0.5 to 30 $\mu$M for 30 min.

Fluorescence quenching of sensor was evaluated through incubation with various biomolecules and ions. Figure 3.6 shows quenching efficiencies 100 $\mu$M of analytes compared to 10 $\mu$M DA. Quenching efficiency of DA was 60% whereas that of other analytes did not exceed 10% despite to their 10-fold more concentration.

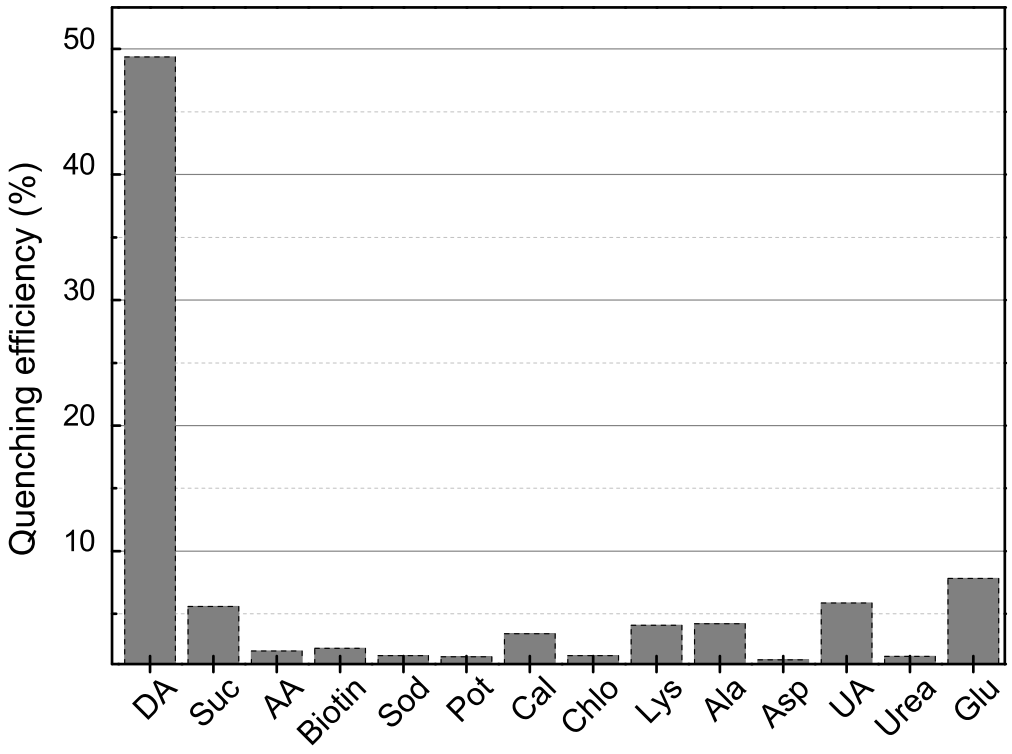


Figure 3.6: Quenching efficiencies after incubated with 10 $\mu$M of DA and 100 $\mu$M of various analytes. Suc: sucrose, AA: ascorbic acid, Sod: sodium ion, Pot: potassium, Cal: calcium ion, Chlo: chloride ion, Lys: lysine, Ala: alanine, Asp: aspartic acid, UA: uric acid, and Glu: glucose.

Quinone which is the oxidized form of dopamine is converted to 5,6-dihydroxyindole (DHI). DHI undergoes oxidation and branching reactions leading to the formation of dimers and oligomers which then self-assemble to form cross-linked polymer called polydopamine (PDA). PDA exhibits broadband monotonic absorption ranging from UV to visible region similarly to eumelanin polymer. In the assay, formation of PDA was shown using absorption spectrophotometry. Initially, only absorption bands of pyrene molecules were observed at 321 and 336

nm (Figure 3.7). After DA addition, a broadband absorption arised in the visible region with a maximum at 400-550 nm . In addition, absorption intensities increased in UV region. Absorption intensity kept increase within time as PDA growth continued.

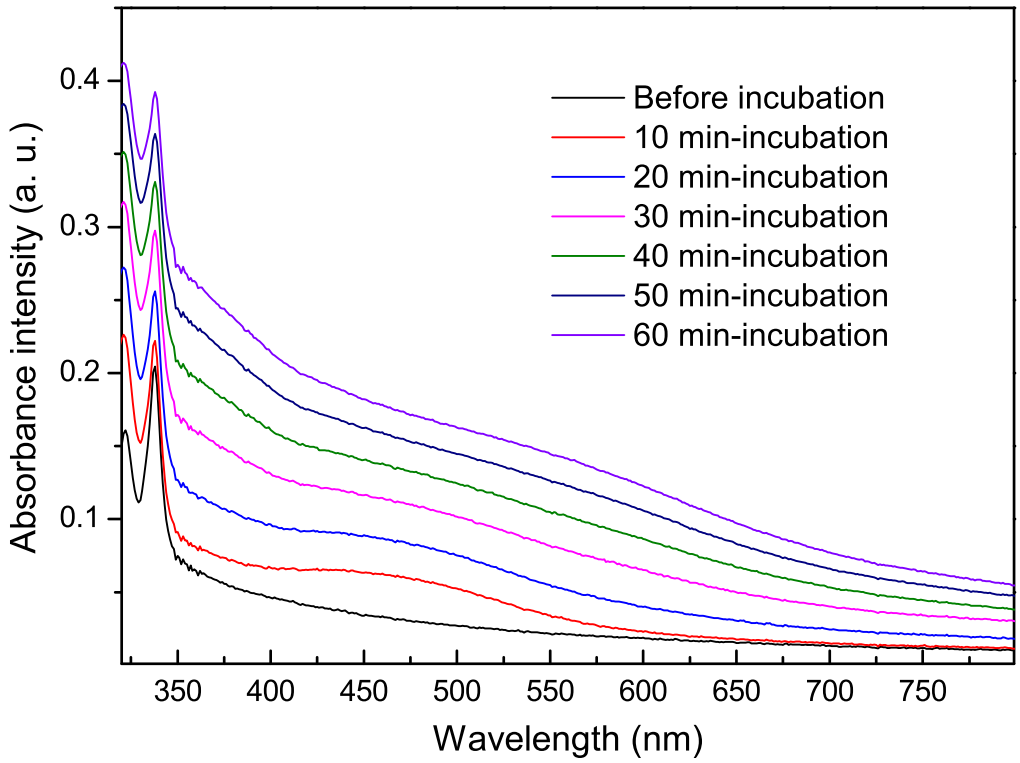


Figure 3.7: UV-visible absorption spectra of the r-pMSNs assay without DA and after incubated with 0.3 mM DA for 10, 20, 30, 40, 50, and 60 min.

PDA has excitation wavelength-dependent emission. For example when excited with 420 nm, PDA exhibits emission at 450-550 nm. To understand quenching mechanism during DA detection, fluorescence was investigated in more detail. r-pMSNs were incubated with 5 mM DA. Initially, r-pMSNs had strong emission since DA was absent as illustrated in (Figure 3.8a top). In the presence of DA, quenching of pyrene emission and formation of weak green PDA emission was

observed under UV light (Figure 3.8a bottom). Additionally, weak green PDA emission was. While initially assay was colorless under visible light it was turned to brown upon incubation with DA due to PDA formation (Figure 3.8b). Figure 3.8c shows r-pMSNs under UV illumination before and after incubation with 25 $\mu$M DA for 30 min. Interestingly, top of solution was darker than middle and bottom regions which indicates higher emission quenching occured at oxygen-rich top region. This result further confirms electron transfer between pyrene molecules and quinone formed from DA in oxygen-rich environment.

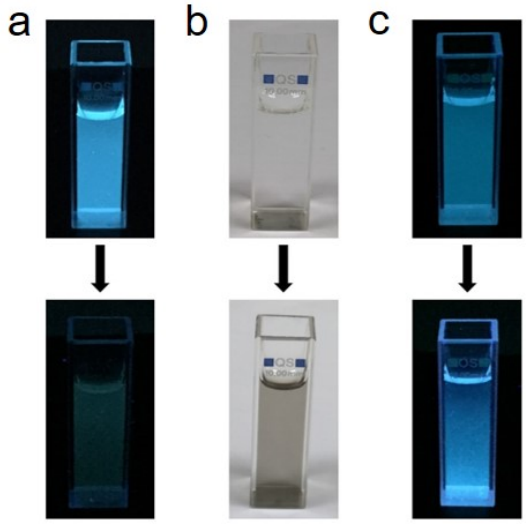


Figure 3.8: (a) UV-illuminated r-pMSNs assay before (top image) and after incubation with 5 mM DA for 30 min (bottom image). (b) Visible light-illuminated r-pMSNs assay before (top image) and after incubation with 5 mM DA for 30 min (bottom image). (c) UV-illuminated r-pMSNs assay before (top images) and after (bottom images) incubation with 25 $\mu$M DA. Brown top part indicates that emission quenching was generated by DA oxidation in oxygen-rich top region.

Hybridization of r-pMSNs with PDA was visually observed under visible light. Figure 3.9a shows 1.2 mg/mL of r-pMSNs assays incubated with 50 $\mu$M, 100 $\mu$M, 500 $\mu$M, and 1 mM DA for 30 min. Brown color became stronger with DA above 50 $\mu$M condition. Formation of brown color at the top of solutions showed PDA formation. Figure 3.9b shows r-pMSNs-PDA hybrid particles centrifuged after incubation. In the presence of 50 $\mu$M, r-pMSNs hybridized with a very thin PDA

layer and further DA increase increased PDA thickness.

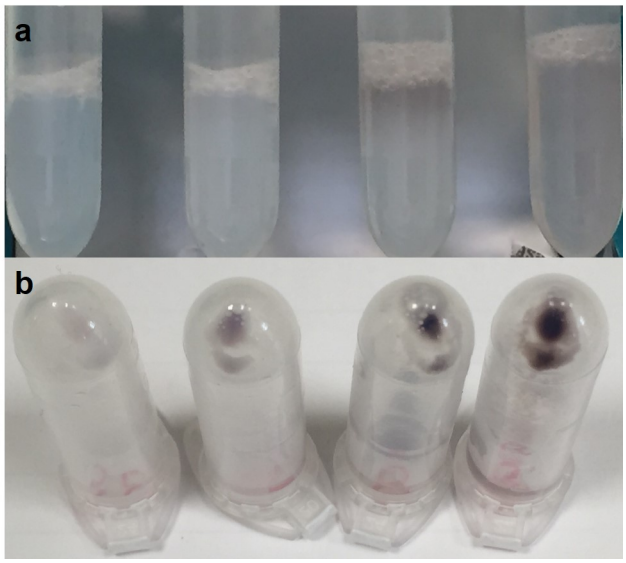


Figure 3.9: a) 1 mL of r-pMSNs assays incubated with 50 $\mu$M, 100 $\mu$M, 500 $\mu$M, and 1 mM of DA (from left to right) for 30 min. b) Centrifuged r-pMSNs-polydopamine (PDA) hybrids formed after incubation of 1 mL of r-pMSNs with 50 $\mu$M, 100 $\mu$M, 500 $\mu$M, and 1 mM of DA (from left to right) for 30 min.

Zeta-potentials of bare r-pMSNs and r-pMSNs-PDA hybrid particles were measured. Figure 3.10 shows the zeta-potential curves obtained from three measurements. Bare r-pMSNs had positive zeta potential around 10.3 mV which was due to positively charged cetyltrimethylammonium (CTA) micelles on nanorod surfaces. Particles became negatively charged with a potential of -23.7 mV after incubation with DA. Negative charge was due to the external PDA layer which is negatively charged in basic pH.

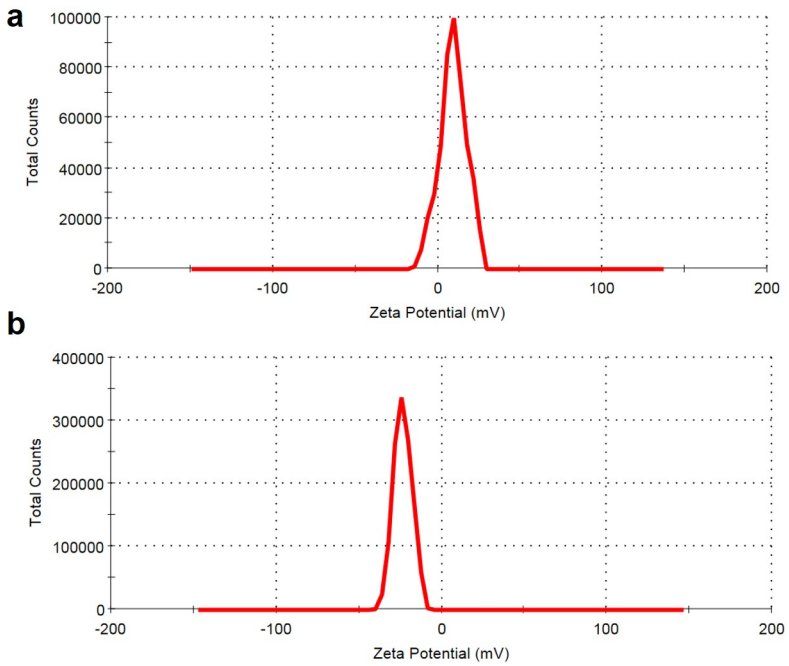


Figure 3.10: Zeta-potential profiles r-pMSNs (a) before and (b) after incubation with 50 $\mu$M of DA for 30 min.

In conclusion, a facile method was developed to prepare pyrene confined rod-shaped mesostructured (r-pMSNs) silica nanoparticles for sensitive detection of dopamine in water. Pyrene was encapsulated in mesostructured nanoparticles through hydrophobic-hydrophobic interactions between CTA micelles and pyrene. Rod-shaped organic/inorganic hybrid nanoparticles had uniform size distribution in water. Bright excimer emission of r-pMSNs exhibited rapid and visual quenching against dopamine.

# Chapter 4

# Two-dimensional Superhydrophilic Patterning on Superhydrophobic Organically Modified Silica (Ormosil) Films

A surface with water contact angle higher than 150° and sliding angle lower than 10° is called superhydrophobic. Such surfaces repel water and droplets roll-off from them easily. On the other hand, a surface which spreads water and has contact angles less than 10° is known as superhydrophilic [55]. Wettability contrast by generating superhydrophilic and superhydrophobic patterns on the same scale is desired for applications such as water harvesting and microfluidics [56–65]. In addition, droplet arrays, droplet manipulation, immobilization of droplet-dispersed materials such as biomolecules are formed as a result of precise tuning of superhydrophilic and superhydrophobic patterns on a single surface [66, 67]. Therefore, surfaces with patterned wettability have attracted great interest for high-throughput biological and chemical screening [68–71]. Numerous methods such as plasma treatment, direct laser writing and ink-printing have been introduced in order to develop patterned surfaces over the past decade

[72–88]. Alternatively, UV/ozone (UV/O) treatment offers a simple way for superhydrophilic patterning. UV/O treatment was also used for the preparation of patterned polymer surfaces [68]. However, contact angle increases on polymer surfaces over time after treatment due to hydrophobic recovery effect and reorganization of polymeric bonds [89–91].

In this thesis, a facile method was developed for generation of very stable superhydrophilic/superhydrophobic patterned surfaces. Superhydrophobic surfaces were prepared from nanostructured ormosil nanoparticles synthesized via sol-gel method. Isolated super-wetted/non-wetted patterns were generated by treating with UV/O on superhydrophobic surfaces. UV/O modifies does not change surface morphology; changes surface chemistry from hydrophobic methyl groups to hydrophilic silanol groups. Super-wetted patterns maintained their wetting performance during several months of storage suggesting their suitability for practical applications. Wettability degree on patterned surface can be precisely tuned depending on UV/O exposure duration. Contact angles (WCA) of generated wetted patterns can be nearly 0° while unmodified regions have WCA of 170°. Droplet arrays can be formed on patterned surfaces by dipping water or microdroplets can be aliquoted to separate superhydrophilic patterns. Wettability difference between untreated and UV/O-treated regions was exploited for bioadsorption. In addition, superhydrophilic-superhydrophobic patterns were strong against bending forces owing to flexible nature of coatings.

## 4.1 Experimental Section

### 4.1.1 Materials

Methyltrimethoxysilane (MTMS), ammonium hydroxide (25%), oxalic acid were purchased from Merck. Methanol was purchased from Carlo-Erba. Fluorescein isothiocyanate-bovine serum albumin conjugate (FITC-BSA) was purchased from Sigma-Aldrich. Deionized (DI) water (18.2 MΩ.cm at 25 °C) was obtained using

a Millipore Milli-Q water purification system (Billerica). All chemicals were used as received.

### 4.1.2 Preparation of superhydrophobic ormosil coatings

Superhydrophobic ormosil coatings were produced using sol-gel reaction method [92]. 1 mL of MTMS was dissolved in 9.74 mL of methanol. 0.5 mL of 1 mM oxalic acid solution was added dropwise and solution was stirred for 30 min. Then, mixture was left to incubate for 24 h to hydrolyze organosilane precursor. Then, 0.19 mL of water and 0.42 mL of ammonia solution (25%) were added and stirred for 15 min. Resultant mixture was aged for 2 days at room temperature to obtain complete gel. After aging step, 9 mL of methanol was added and homogenized using an ultrasonic sonicator probe for 45 s at 20 W. 250 mL-portions of formed colloidal ormosil solution were deposited onto clean quartz or glass substrates (1x2 cm) using spin-coater operating at 3000 rpm.

### 4.1.3 Preparation of superhydrophilic patterns

Superhydrophobic ormosil coatings were covered with cellulose acetate sheets which were previously hollowed at pre-defined areas using a 30 W $CO_2$ laser cutting system (Epilog Zing). Then, surfaces were exposed to UV/O for durations varying from 5 to 60 min using a surface cleaning system (PSD-UV, Novascan Technologies) at ambient temperature. Power intensity was 8 mW/cm$^2$ and 30 mW/cm$^2$ for 185 nm and 253.7 nm wavelengths, respectively.

### 4.1.4 Selective protein and bacteria adsorption on wetted patterns

Arrays of circular patterns (with 1 mm diameter) with varying degrees of wettability were generated on superhydrophobic surfaces by varying UV/O exposure

time (15, 30 and 60 min). As-prepared microchips were then soaked into 1 mg/ml FITC-BSA aqueous solution for 30 s and then gently washed with DI water to remove non-adsorbed proteins. For cell adsorption studies, 2 $\mu$m sized E. coli bacteria which have GFP (green fluorescent protein) were used. Microdroplets of bacteria suspension were aliquoted on square-shaped wetted patterns by rolling 200 $\mu$L of bacteria suspension over surfaces.

### 4.1.5 High-throughput droplet mixing on patterned surfaces

Arrays of circular wetted patterns (0.5 mm diameter) were generated on two separate superhydrophobic surfaces. Droplet arrays were then generated on patterned surfaces by rolling blue-dyed and red-dyed large droplets over them. Patterned surfaces were aligned on a microstage with droplet holding sides facing each other. Then, droplets were mixed by approaching separate surfaces with the help of microstage motor.

### 4.1.6 Characterization

Surface morphology of surfaces was analysed with scanning electron microscope (E-SEM, Quanta 200F, FEI) under high vacuum condition at 10 kV after coating surfaces with 6 nm-thick gold/platinum layer. Chemical analysis of patterns was performed using X-ray photoelectron spectroscopy (Thermo Fisher Scientific). Avantage software was used for peak identification and fittings. Static water contact angles (WCA) of patterns were measured using a contact angle meter (OCA 30, Dataphysics) and 4 $\mu$L of water droplets. Fluorescent images of protein-adsorbed patterns were taken with confocal microscope (Model LSM 510, Zeiss) using 10X objectives. Argon laser was used for excitation at 488 nm. Emission at 505 nm was collected. Droplet capture on superhydrophilic patterns was recorded using a high-speed camera (Phantom Miro M310, Vision Research) operating at 2000 fps.

## 4.2 Results and Discussion

Robust superhydrophilic patterned superhydrophobic coatings were developed for high-throughput biomolecular adsorption and droplet mixing. Superhydrophobic coatings were produced from organically modified silica (ormosil) nanoparticles synthesized via sol-gel method. Superhydrophilic patterns were generated on prepared surfaces using UV/O treatment step. SEM image of ormosil surface revealed highly porous structure (Figure 4.1a). A static water contact angle (WCA) of 170° was measured as a result of roughness and low energy methyl groups (inset of Figure 4.1a). UV/O treatment decomposed hydrophobic moieties and contact angle decreased nearly 0° (Figure 4.1b). Porous surface structure of treated coatings remained intact upon treatment.

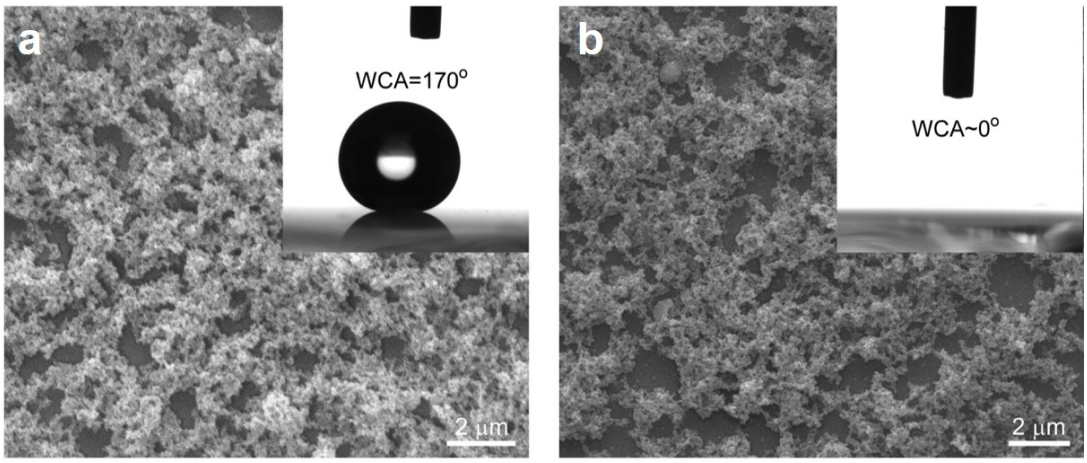


Figure 4.1: a) Scanning electron microscopy (SEM) image of superhydrophobic organically modified (ormosil) coating with water droplet profile in the inset. b) SEM image of 1 h UV/ozone-treated surface with spreading droplet in the inset.

X-Ray photoelectron spectroscopy (XPS) was used to analyse surface chemistry after UV/O treatment. Untreated ormosil surface structure was composed of approximately 37.3% oxygen, 20.6% carbon and 42.1% silicon while chemical composition of 1 h-treated surface was 51.9% oxygen, 6.3% carbon and 41.8% silicon (Figure 4.2). Ozone and reactive atomic oxygen atoms produced by UV light (185 nm and 254 nm) cleave low energy surface-bound hydrocarbons leading

to oxygen enrichment and formation of hydroxyl ($OH^-$) groups [93, 94].

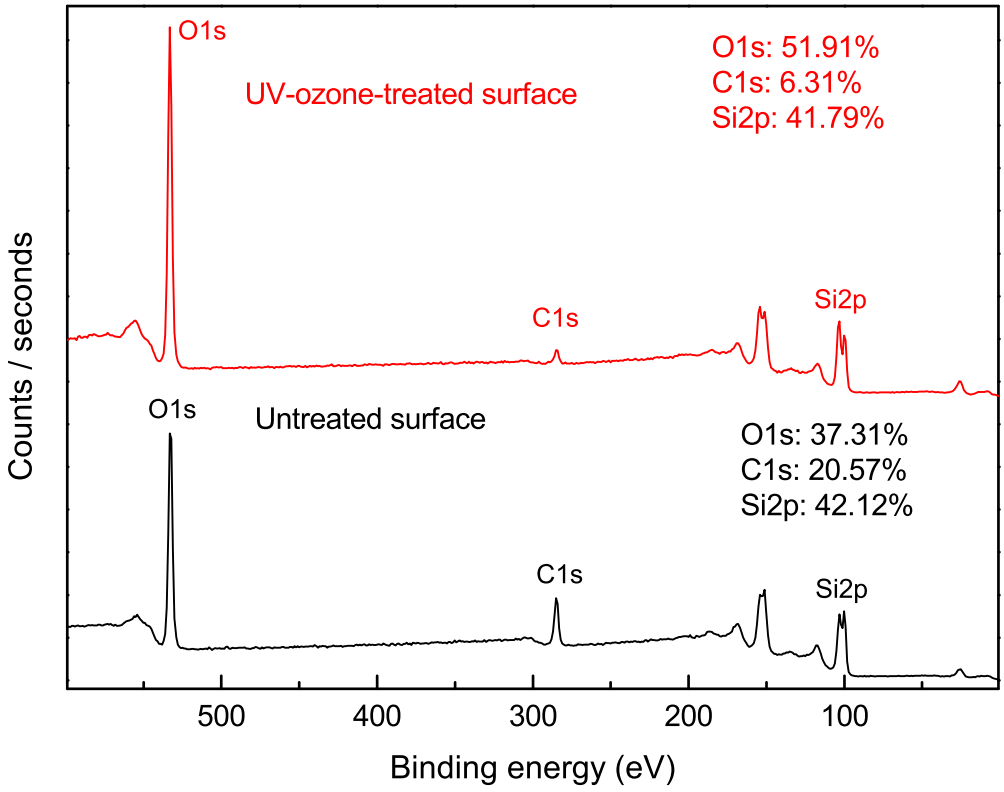


Figure 4.2: X-ray photoelectron spectroscopy (XPS) survey spectra of UV/ozone-treated and untreated ormosil surfaces.

Control of degree of wettability from superhydrophobic to superhydrophilic is desired for precise liquid transport and droplet handling [68]. Wettability can be precisely controlled on ormosil coatings from superhydrophobic to superhydrophilic with WCA ranging from 170° to 0° depending on UV/O treatment time. WCA decreased linearly with increasing UV/O exposure time. Extreme wettability (WCA $\simeq 0°$) was obtained upon treatment for 45 min (Figure 4.3). Water droplet shape turned from spherical to hemispherical within 20 min, then to a thin liquid film upon 45-60 min treatment.

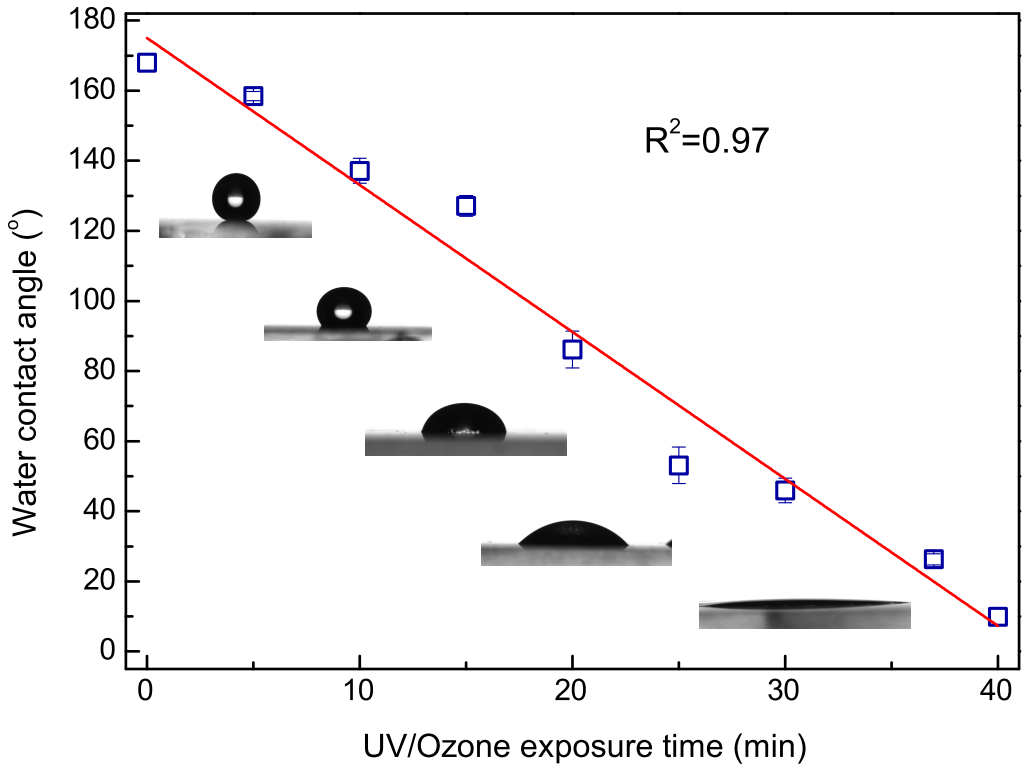


Figure 4.3: Change of water contact angles on UV/O-exposed ormosil surfaces depending on treatment time. Intensities are averages of three repeated measurements. Error bars show standard deviation. Inset images represent droplet profiles captured for 0, 5, 10, 20, 30 and 40 min treatment times from top to bottom.

Masked UV/O illumination was utilized to create wetted micropatterns on superhydrophobic ormosil coatings (Figure 4.4a). As-prepared superhydrophobic coatings were treated with UV/O for 60 min through shadow masks placed on coatings. Regions under hollow sites of masks became selectively modified by UV/O whereas remaining regions were protected from UV. Droplet conserved its sphere shape on untreated region due to unaffected chemical groups whereas colored solution spreading on treated area shows wetting property (Figure 4.4b).

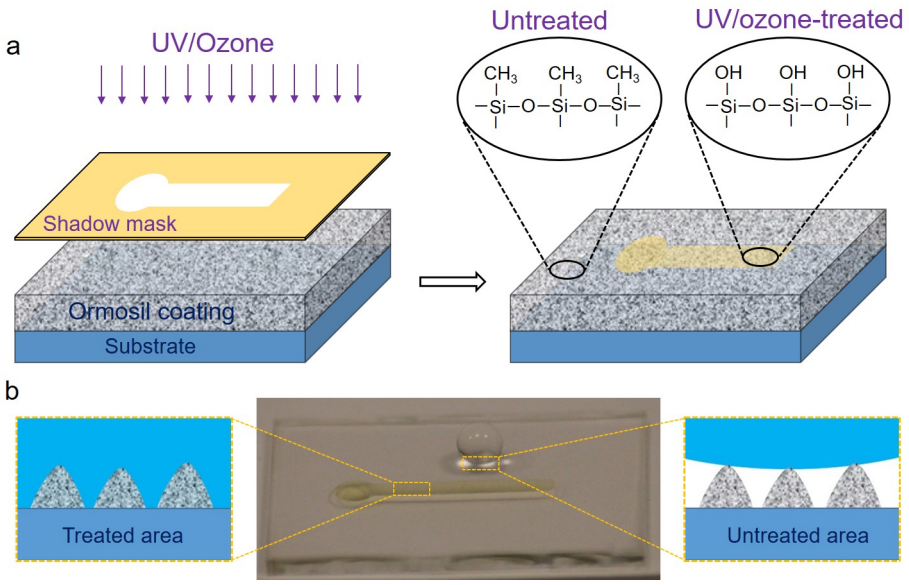


Figure 4.4: a) Schematic representation of UV/O treatment (left) and chemical groups on treated and untreated areas (right). b) Photo and schematic of patterned surface with completely spreading fluorescein isothiocyanate-bovine serum albumin conjugate (FITC-BSA) solution on superhydrophilic area and spherical water droplet sitting on superhydrophobic area. Schemes represent wetting and Cassie state non-wetting.

Well-defined wetted patterns with various size and shapes including square, stripe and circle were formed using different mask designs (Figure 4.5). Multiplexed analysis can be performed on patterned microchips since one can individually aliquot various aqueous components to distinct superhydrophilic spots (Figure 4.5a). High density droplet microarrays can also be generated on patterned surfaces by dipping into aqueous solutions or by rolling a large droplet over surfaces (Figure 4.5c). Furthermore, superhydrophilic and superhydrophobic patterns remained stable when bending was applied owing to flexible ormosil that preserves its structure under mechanical stress (Figure 4.5d) [95].

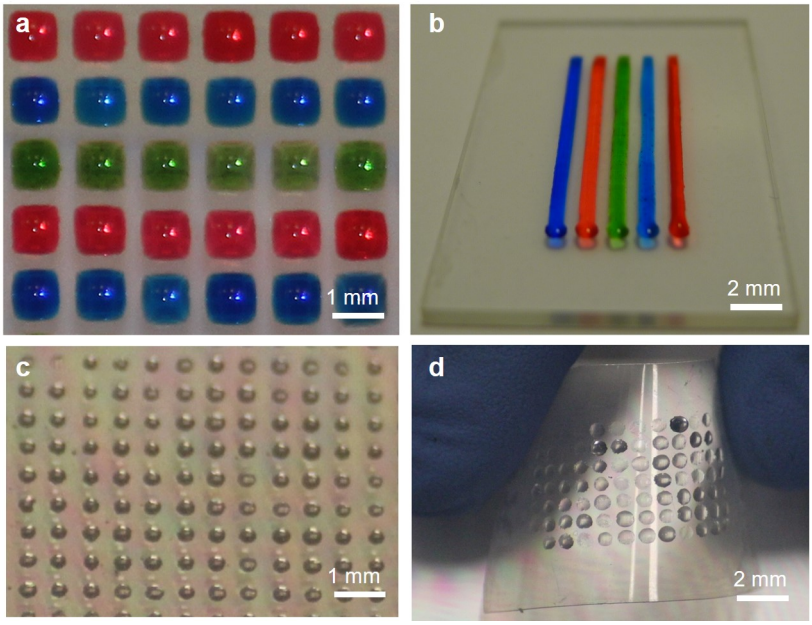


Figure 4.5: a) Ormosil surface with square-shaped super-wetted patterns holding different colored droplets (each squared pattern edge is 1 mm). b) Ormosil surface on glass substrate with colored droplets in stripe patterns with 1 mm width (Blue dye is methylene blue, red dye is rhodamine 6G, and green dye is mixture of acridine orange and methylene blue). c) High-density droplet array in 200 $\mu$m-sized circular patterns. d) Patterned ormosil surface on a bent cellulose acetate sheet and droplet array formed on patterns.

Formation of droplet arrays was recorded using a high-speed camera operating at 2000 fps on a patterned surface with 200 $\mu$m-sized wetted spots (Figure 4.6). Upon rolling large droplet over tilted surface, small droplets were distributed to isolated spots.

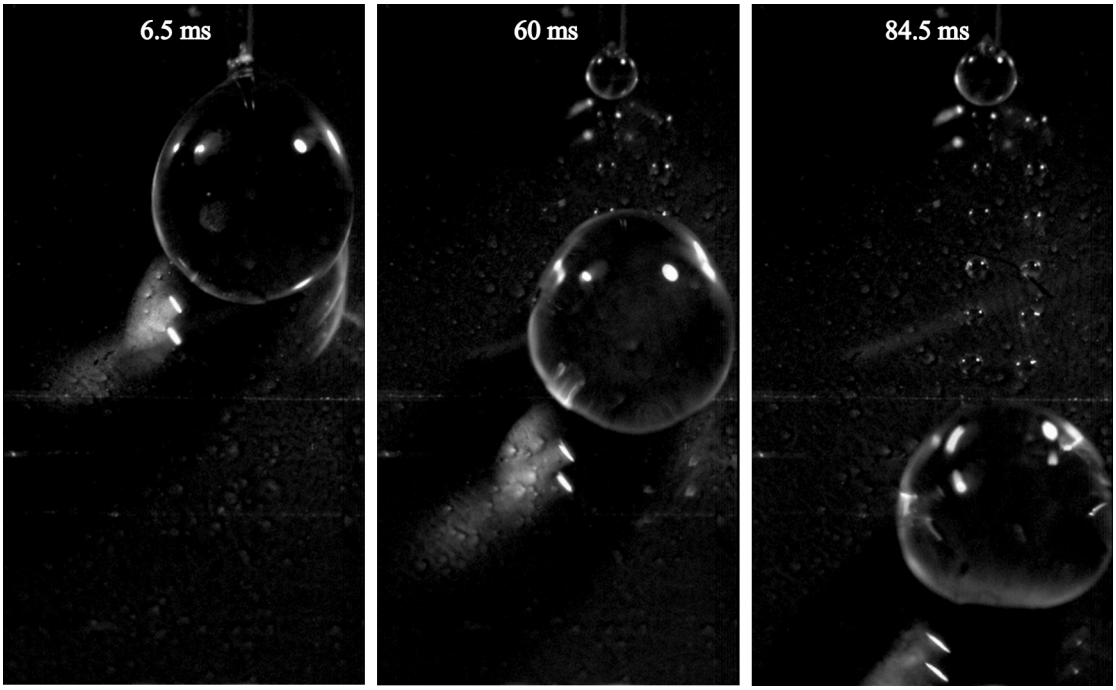


Figure 4.6: Snapshots from high-speed video recording of droplet movement at 6.5th, 60th, and 84.5th milliseconds (ms) for the surface with 200 $\mu$m circular patterns.

Time-dependent stability of superhydrophilic/superhydrophobic patterns is important for long-life analysis platforms. Accordingly, contact angles of patterned surfaces were measured after 5 month-storage at ambient conditions. No remarkable change was observed in WCA confirming the robustness of patterns during long storage periods (Figure 4.7).

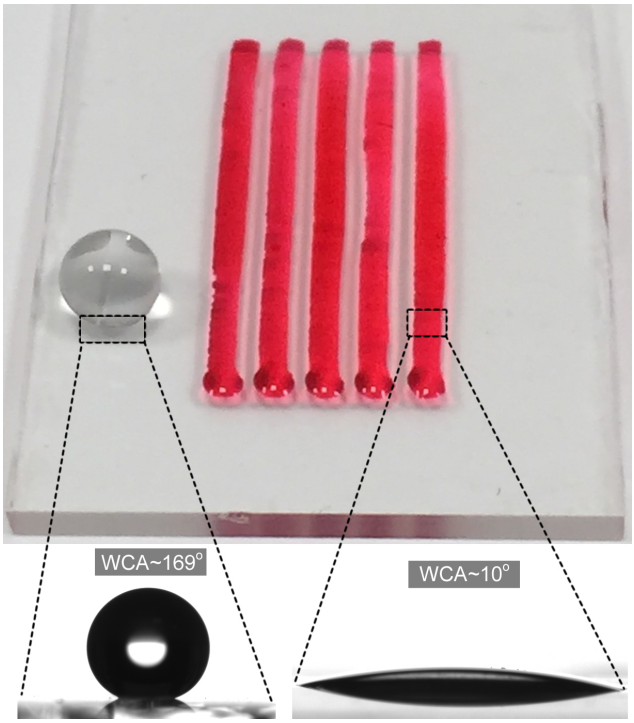


Figure 4.7: Patterned ormosil surface after 5 month-storage period. Spherical droplet on a superhydrophobic region and rhodamine 6G solution on superhydrophilic stripe patterns with corresponding water contact angles.

In order to demonstrate high-throughput biomedical screening, FITC-BSA were deposited on wetted patterns. Fluorescent signal was observed on patterns while no signal was observed on untreated regions revealing selective adsorption on patterns (Figure 4.8). Furthermore, concentration of FITC-BSA increased with increasing UV/O treatment time as revealed with increasing fluorescence (Figure 4.9).

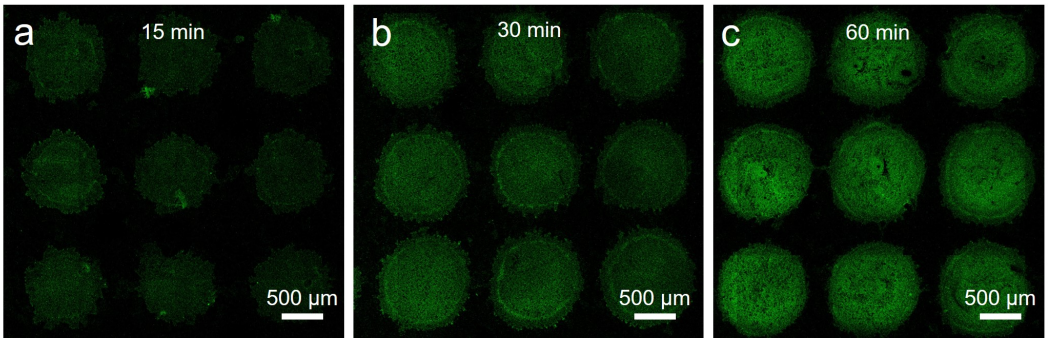


Figure 4.8: Fluorescent images of BSA-adsorbed patterns prepared via UV/O treatment for (a) 15 min, (b) 30 min and (c) 60 min. Green fluorescent corresponds to FITC emission which is conjugated with BSA whereas black background corresponds to superhydrophobic regions with no adsorbed BSA.

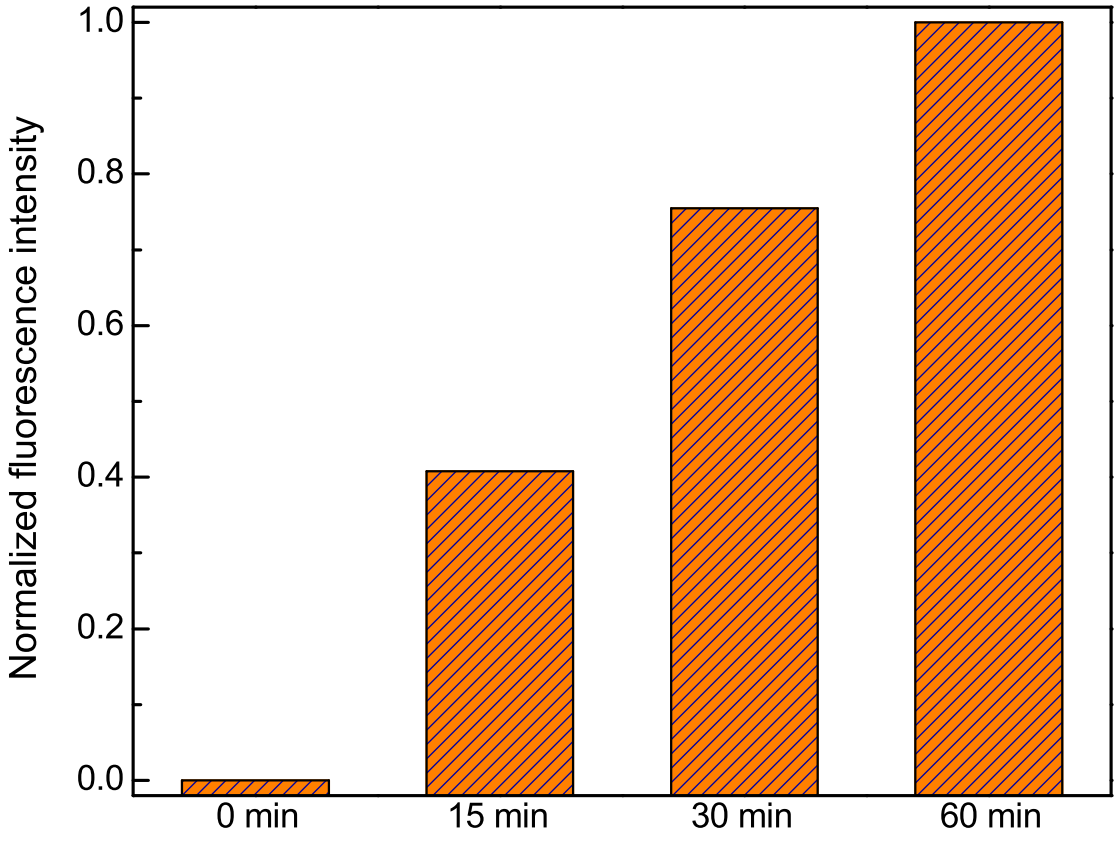


Figure 4.9: Normalized fluorescence intensities with respect to UV/O treatment time. Intensities were calculated from confocal images shown in Figure 4.8.

Adsorption of GFP-expressing E. coli was shown on square-shape superhydrophilic patterns. Fluorescent signal of GFP with 2 $\mu$m dimensions was observed only in superhydrophilic patterns revealing good confinement of bacteria cells in wetted areas (Figure 4.10). High-throughput mixing was also demonstrated on patterned surfaces using droplet arrays produced with two different contents (Figure 4.11).

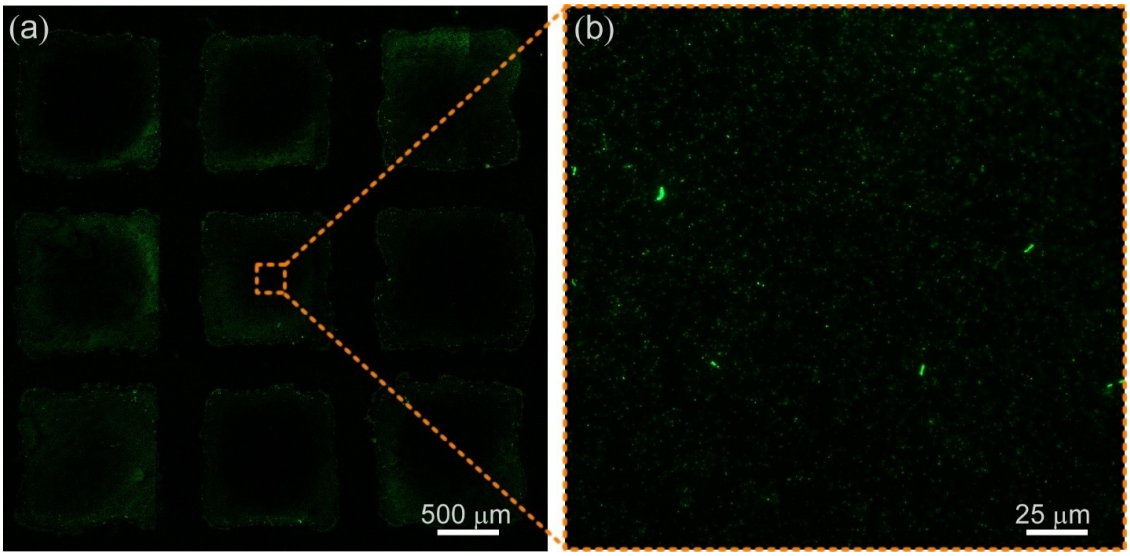


Figure 4.10: (a) Fluorescent microscope image of green fluorescent protein (GFP)-expressing E. coli cells on 1 mm-sized wetted patterns. b) Close-up view of one wetted pattern with adhered bacteria.

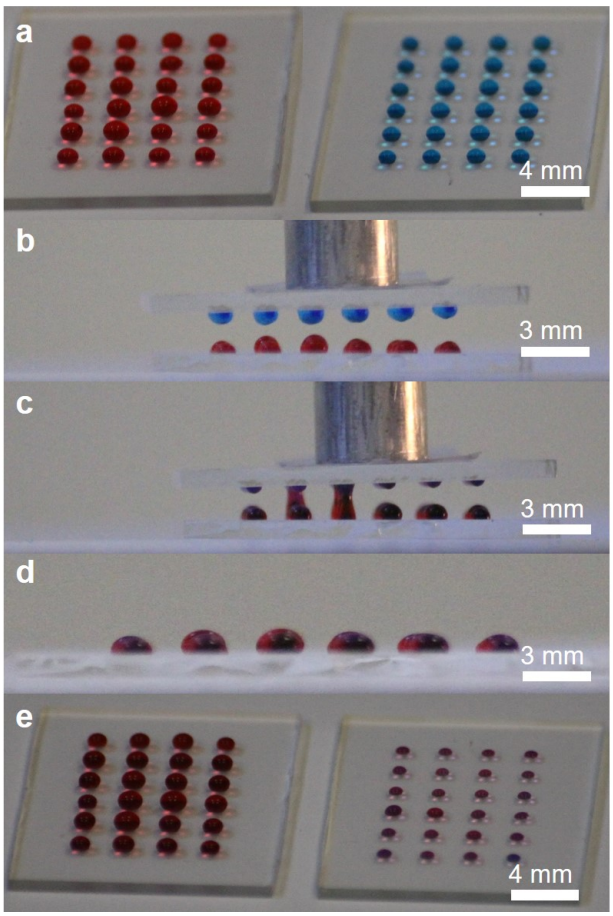


Figure 4.11: High-throughput mixing of individual droplets on patterned ormosil surfaces. a) Colored droplet arrays (blue dye is methylene blue and red dye is rhodamine 6G) on two separate surfaces. Identical array sizes (a 4x6 array) were used. b) Patterned surfaces aligned using a microstage. c-d) Droplet arrays during and after contact. Each individual droplet on the top surface mixed with its counterpart at the bottom surface. No lateral mixing was observed between the droplets. e) Arrays of mixed droplets.

Superhydrophilic patterning on superhydrophobic ormosil surfaces was demonstrated. UV/O treatment on selected areas of ormosil surface leads to the formation of very stable superhydrophilic patterns without changing surface morphology. Super-wetted patterns can capture any water-soluble materials which can be used for high-throughput molecular screening.

# Chapter 5

# Droplet-based Glucose Detection on Superhydrophilic-Patterned Surfaces

Superhydrophobic surfaces patterned with well-defined wetted patterns have been important for high-throughput biological and chemical screening inside droplets placed on top since they provide enhanced reaction rates and sensing signals [96]. Micro-scale droplets are confined on superhydrophilic patterns due to wetting contrast between hydrophilic patterns and hydrophobic areas [97]. Upon evaporation of droplets, substances dispersed in droplets enrich which increases molecular interaction frequencies (Figure 5.1). Such an enrichment effect increases reaction rates providing enhanced detection signals whereas signals remain too low to be detected in dilute samples [98].

A few reports have demonstrated detection of DNA, RNA, protein and bacteria inside stationary droplets by exploiting high sensitivity advantage of evaporation-induced enrichment effect [99–103]. To obtain a practical platform for droplet-based assays, superhydrophobic organically modified silica coated surfaces with circular superhydrophilic patterns generated via UV/Ozone treatment (described in Chapter 4) were used. Two-dimensional chemical patterning without physical

decomposition resulted in isolation of aqueous droplets in small wetted spots (Figure 5.1). These surfaces provide a very strong contrast between wetting and non-wetting regions. Additionally, they can be generated with high precision and they are suitable for large area processing and stable at a wide range of temperature [104]. In this thesis, versatility of these surfaces was shown using a novel glucose assay.

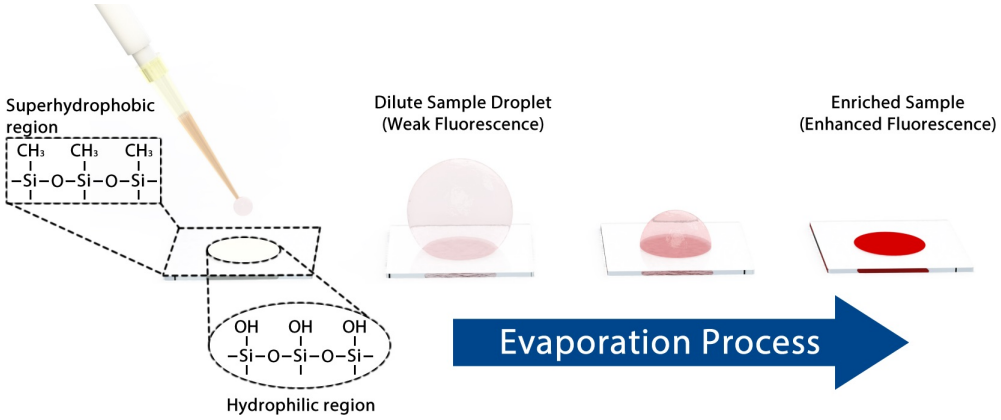


Figure 5.1: Schematic representation of droplet pinning on superhydrophilic circular pattern of a superhydrophobic ormosil surface and evaporation-induced enrichment of low concentration fluorescent sample and resulting fluorescence enhancement.

Perez et al. recently have developed a micropillar-based platform and have shown that 2.5 mM glucose can be detected in evaporating droplets placed on pillars. They used horseradish peroxidase (HRP)/glucose oxidase (GOx)/chromogen as the sensing probe [105]. However, HRP has some drawbacks such as high cost and instability. Therefore, various peroxidase mimicking nanomaterials have been introduced including quantum dots, metal nanocluster and dyes [106–108]. Conjugated polymers have been also used as peroxidase mimicking nanomaterials based on direct or indirect interactions between hydrogen peroxide ($H_2O_2$) and polymer backbones [109–111]. Although such materials exhibit high sensitivity for glucose detection, they usually involve complicated synthesis steps and toxicity. Contrary to these materials, polydopamine can be

easily produced through oxidation and self-polymerization of dopamine in alkaline environments [112]. Particularly, polydopamine fluorescence has recently found applications in bioimaging and dopamine sensing [113–115].

In this thesis, fluorescent polydopamine (PDA) was used for droplet-based glucose sensing probe, for the first time. A sensitive glucose assay was prepared by combining the advantages of PDA such as biocompatibility and ease-of-production with analyte/product enriching capability of patterned organically modified silica (ormosil) surfaces. PDA fluorescence is known to enhance due to decomposition of its aggregated structure by $H_2O_2$. Accordingly, PDA was exploited as glucose probe since $H_2O_2$ is produced in GOx reaction. PDA was first produced from dopamine and incubated with glucose/GOx inside micro droplets placed on wetted patterns. After droplet evaporation, aggregated PDA on patterns radiated bright fluorescence which was observed to increase with increasing glucose concentration. On the other hand, when incubated in mL-volume bulk solution, no significant fluorescence enhancement was obtained within the same time ($\sim$1 h). Fast fluorescence enhancement and stronger signals on patterns revealed increase of reaction rate and sensitivity in evaporating droplets.

## 5.1 Experimental Section

### 5.1.1 Materials

Glucose, sodium hydroxide and hydrochloric acid were purchased from Merck. Glucose oxidase, dopamine hydrochloride, tris(hydroxymethyl)aminomethane, and phosphate buffered saline (PBS) tablets were purchased from Sigma-Aldrich. All chemicals were used as received.

### 5.1.2 Preparation of buffer solutions

10 mM PBS buffer was prepared by dissolving 1 PBS tablet in 200 mL of deionized water and solution pH was adjusted to 7.4 using 1 M sodium hydroxide solution. 50 mM tris solution was prepared and its pH was adjusted to 8.6 using 2 M hydrochloric acid.

### 5.1.3 Glucose assay

2 mL of PBS solutions (pH=7.4) including glucose with concentrations varying from 1 mM to 50 mM were mixed with 50 $\mu$L of 1 mg/mL GOx solution. 20 $\mu$L portions of the mixtures were drop-cast onto separate super-wetted spots of patterned surfaces. Glucose was incubated with GOx at 37 °C for 30 min for complete glucose oxidation. For bulk assay, solutions were also incubated at 37 °C for 30 min. Then, dopamine in tris-HCl buffer (pH=8.6) with a final dopamine concentration of 0.5 mM was added to the glucose/GOx mixtures. For droplet assay, 20 $\mu$L portions of dopamine were added and incubated until droplets completely evaporated which took approximately 50 min. The assay time is a function of the hydrophilic spot size, droplet size and evaporation rate which should be optimized for any given assay. For bulk assay, dopamine and glucose-GOx mixtures were incubated at 37 °C up to 5 h. A control sample containing GOx enzyme without glucose was also prepared and incubated as all other samples.

### 5.1.4 Glucose detection experiments

Fluorescence intensities of droplet-based and mL-scale glucose assays were analyzed using UV light (366 nm, 8W, CAMAG) and fluorescence spectrophotometer (Horiba, Fluorolog®-3, 450 W) by exciting samples at 400 nm and collecting intensities within 420-600 nm range.

## 5.2 Results and Discussion

A droplet-based glucose analysis platform was developed using robust, versatile and low-cost superhydrophilic-patterned silica-based superhydrophobic surfaces. Super-wetted spots with diameter of 0.9 mm or 1.4 mm were generated on as-prepared superhydrophobic surfaces using UV/ozone treatment (described in Chapter 4). Extreme wettability difference between untreated and UV/ozone-treated regions led to confinement of micro droplets and solute substances on small wetted patterns while droplets were repelled from untreated area due to superhydrophobicity (Figure 5.2).

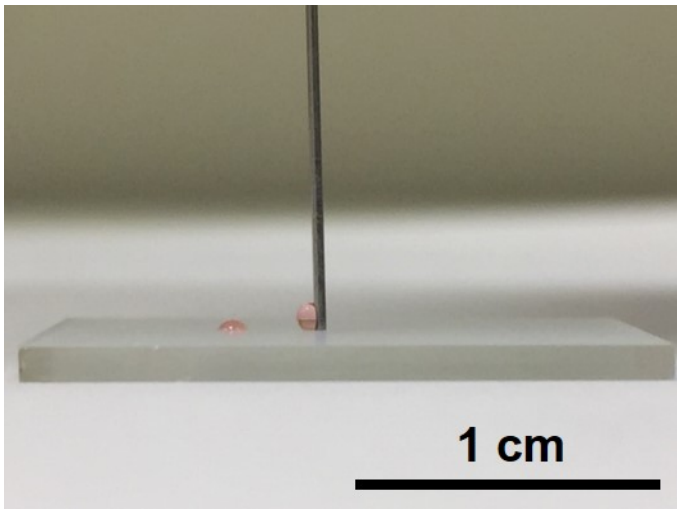


Figure 5.2: Water droplet dyed with ponceau 4R, a food additive, on wetted spot and non-wetted region of patterned surface. Droplet was confined on the wetted area whereas it was repelled from non-wetted part (on the tip of needle) and conserved its spherical shape due to low surface energy.

To obtain evaporation-induced droplet confinement, time-dependent contact angle on a pattern was measured. A 20 $\mu$L droplet drop-cast onto pattern was initially quasi-spherical due to superhydrophobicity of surrounding pattern (Figure 5.3). Upon evaporation, contact angle gradually decreased and droplet finally evaporated.

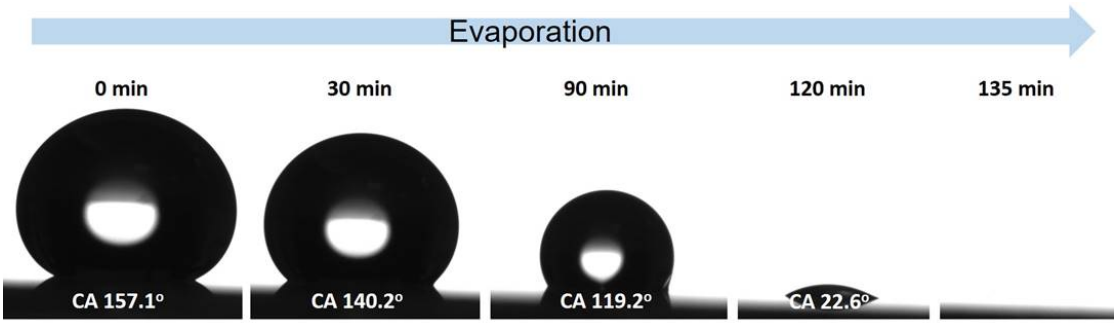


Figure 5.3: Time-dependent contact angle profile of a water droplet on superwetted pattern at room temperature.

PDA which is formed through oxidation and polymerization of dopamine, yields weak green broadband fluorescence within wavelength range from 430 nm to 600 nm (Figure 5.4). Dopamine oxidation produces oligomers which self-assemble and form PDA through $\pi$-$\pi^*$ stacking interactions [112, 116]. Increased interactions result with aggregation-induced quenching in the course of time (Figure 5.4) [117].

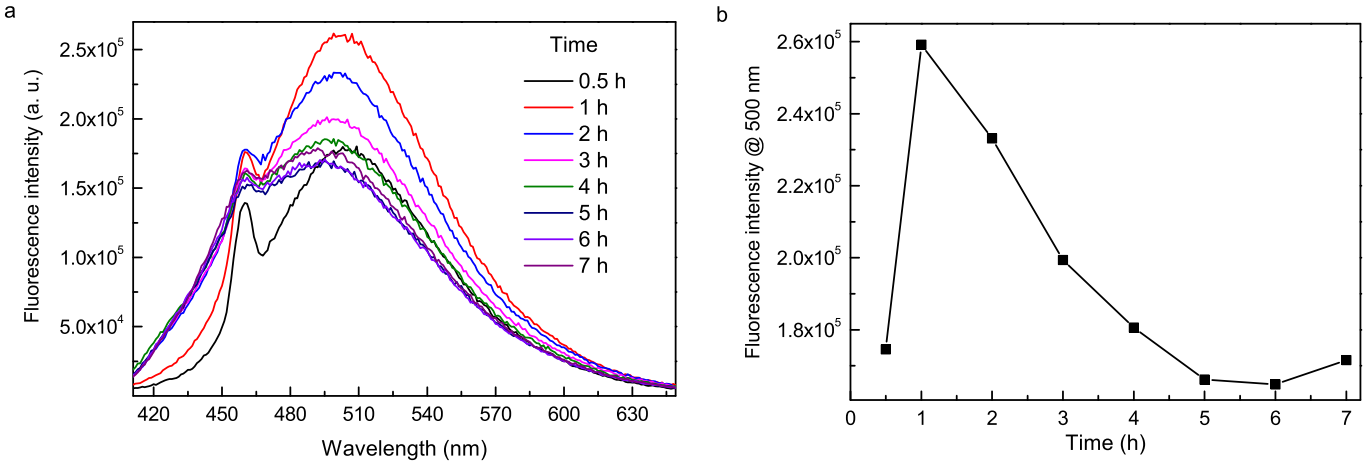


Figure 5.4: Time-dependent fluorescence spectra of polydopamine (PDA) produced from dopamine in basic solution (pH= 8.6). PDA radiates a weak green fluorescence which is increased within first 1 h of growth and then quenched due to $\pi$-$\pi^*$ stacking-induced aggregation of PDA chains in the course of time. b) Fluorescence intensities at 500 nm plotted with data in (a).

When treated with hydrogen peroxide ($H_2O_2$), PDA fluorescence is found to turn on due to decomposition of large PDA polymer aggregates to smaller clusters by hydrogen peroxide [118–120]. Figure 5.5 shows fluorescence increase of PDA when incubated with $H_2O_2$.

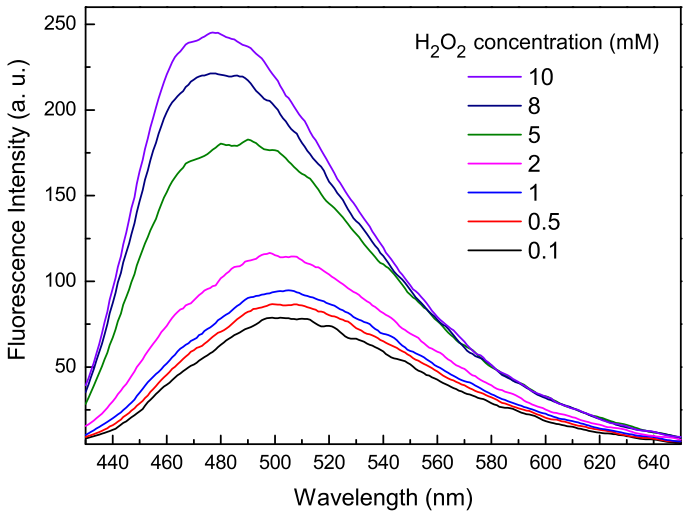


Figure 5.5: a) Fluorescence spectra of PDA with $H_2O_2$ concentration ranging from 0.1 mM to 10 mM after 2 h-incubation with 0.5 mM dopamine in tris buffer.

PDA fluorescence was used for glucose analysis by measuring $H_2O_2$ generated through glucose oxidation. PDA was incubated with glucose solution with concentration ranging from 1 mM to 50 mM in 20 $\mu$L of droplets. Fluorescence intensities were recorded after droplets evaporated which took approximately 50 min at 37 °C. Since glucose was incubated with glucose oxidase enzyme for 30 min before incubation with PDA, total analysis time was 80 min. After incubation and complete droplet evaporation, fluorescent PDA spots were obtained. PDA fluorescence increased with increasing glucose concentration (Figure 5.6).

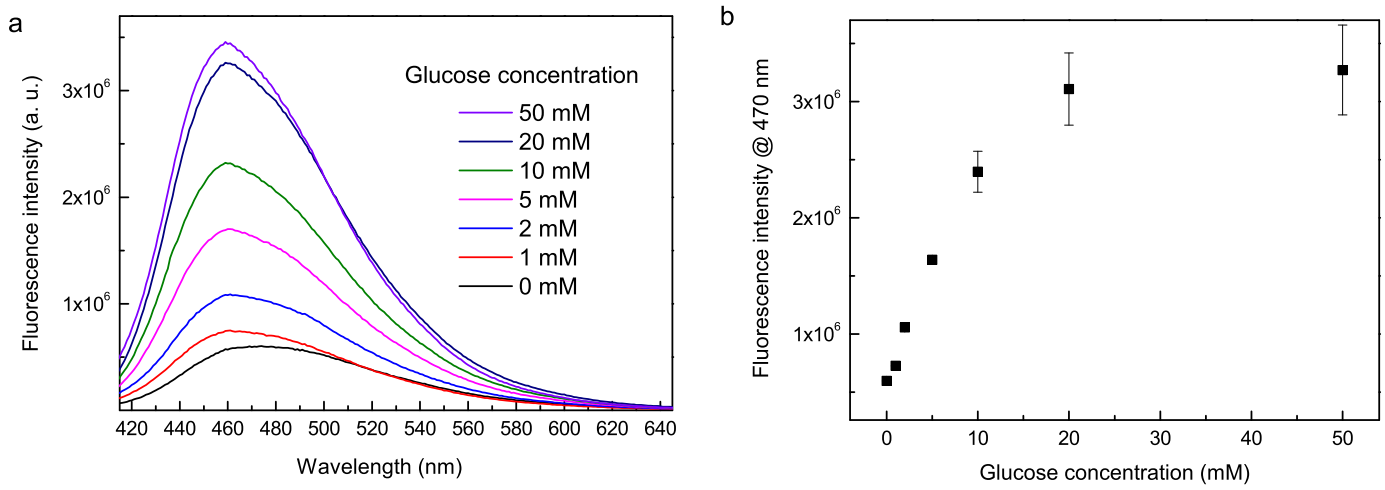


Figure 5.6: a) Fluorescence spectra of PDA incubated with glucose with concentration ranging from 1 mM to 50 mM in evaporating micro droplets on wetted patterns. b) Fluorescence intensities at 470 nm plotted with data in (a). Intensities are averages of three repeated measurements. Error bars show standard deviation.

Furthermore, enhancement of PDA fluorescence was also observed by naked eye under UV light (Figure 5.7). Interestingly, fluorescence was shifted to blue (470 nm) in the presence of glucose concentration above 5 mM revealing reduction of nanoaggregate size with gradual increase of $H_2O_2$ [121]. Limit of detection of fluorescence-based glucose assay was calculated to be 130 $\mu$M using linear calibration curve plotted (Figure 5.8).

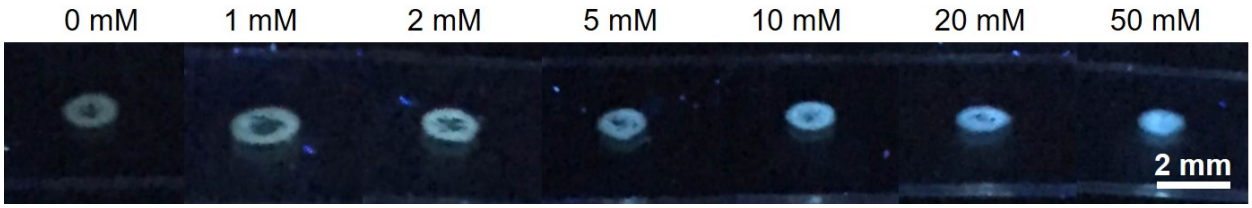


Figure 5.7: a) Photographs of fluorescent PDA spots excited by UV light (366 nm) after incubation with glucose in evaporating droplets.

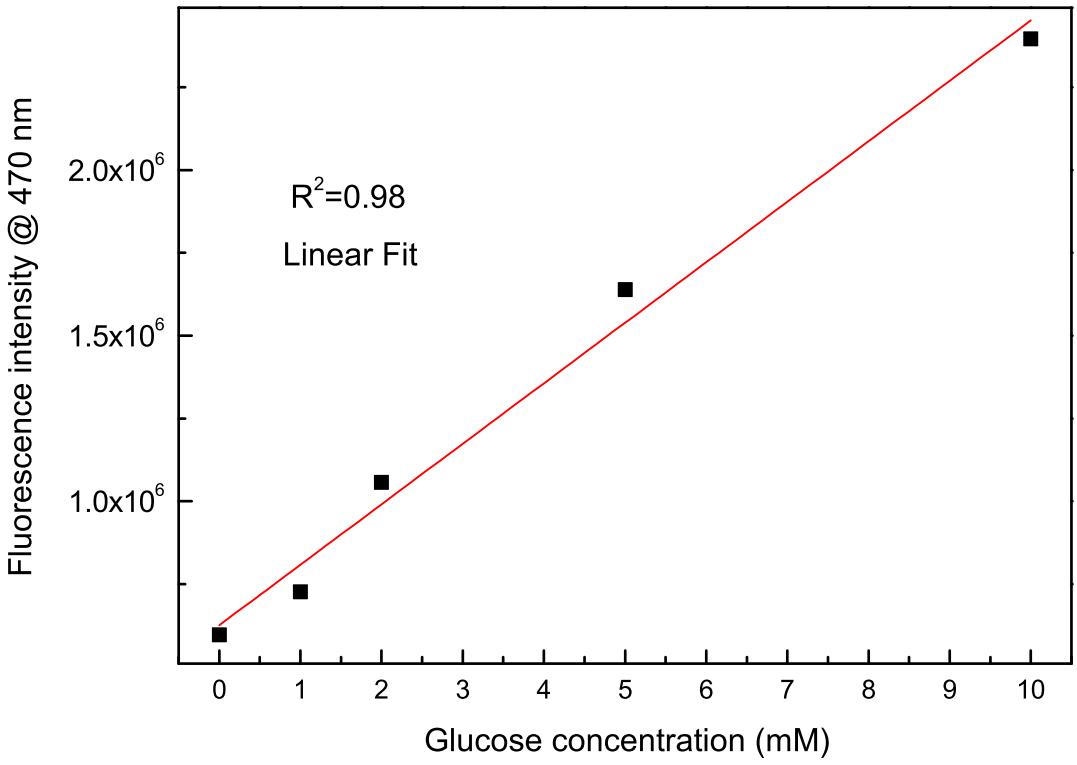


Figure 5.8: a) Linear calibration curve within range from 1 mM to 10 mM glucose concentration. Linear curve with the highest regression coefficient ($R^2$=0.98) was plotted with the lowest five concentration values.

Although fluorescence enhancement was also observed in bulk liquid where insignificant evaporation occurs, the reaction was much slower. To investigate the same reaction in bulk, fluorescence intensities were recorded after incubating PDA with glucose/GOx in 4 mL of buffer solutions for varying durations. Figure 5.9 shows time-dependence of fluorescence intensity at 500 nm. During initial stages of PDA growth, dopamine emission centered at 460 nm was observed besides to PDA emission centered around 500 nm and then gradually disappeared. Fluorescence enhancement was not observed with increasing glucose concentration up to 3-4 h. Upon incubation for 4 h, assay showed sensitivity for concentration range

from 1 mM to 20 mM. This result can be explained by the inhibition of PDA nanoclusters initially when $H_2O_2$ amount was high and then reorganization of nanoclusters through $\pi$-$\pi^*$ stacking interactions in the course of time. Droplet-based assay, accelerated reaction between PDA and $H_2O_2$ and reduced required time to generate fluorescent enhancement to 1 h for wide range of glucose varying from 1 mM to 50 mM. Furthermore, shift of fluorescence maximum was not observed in the bulk liquid revealing the inefficient interaction with $H_2O_2$.

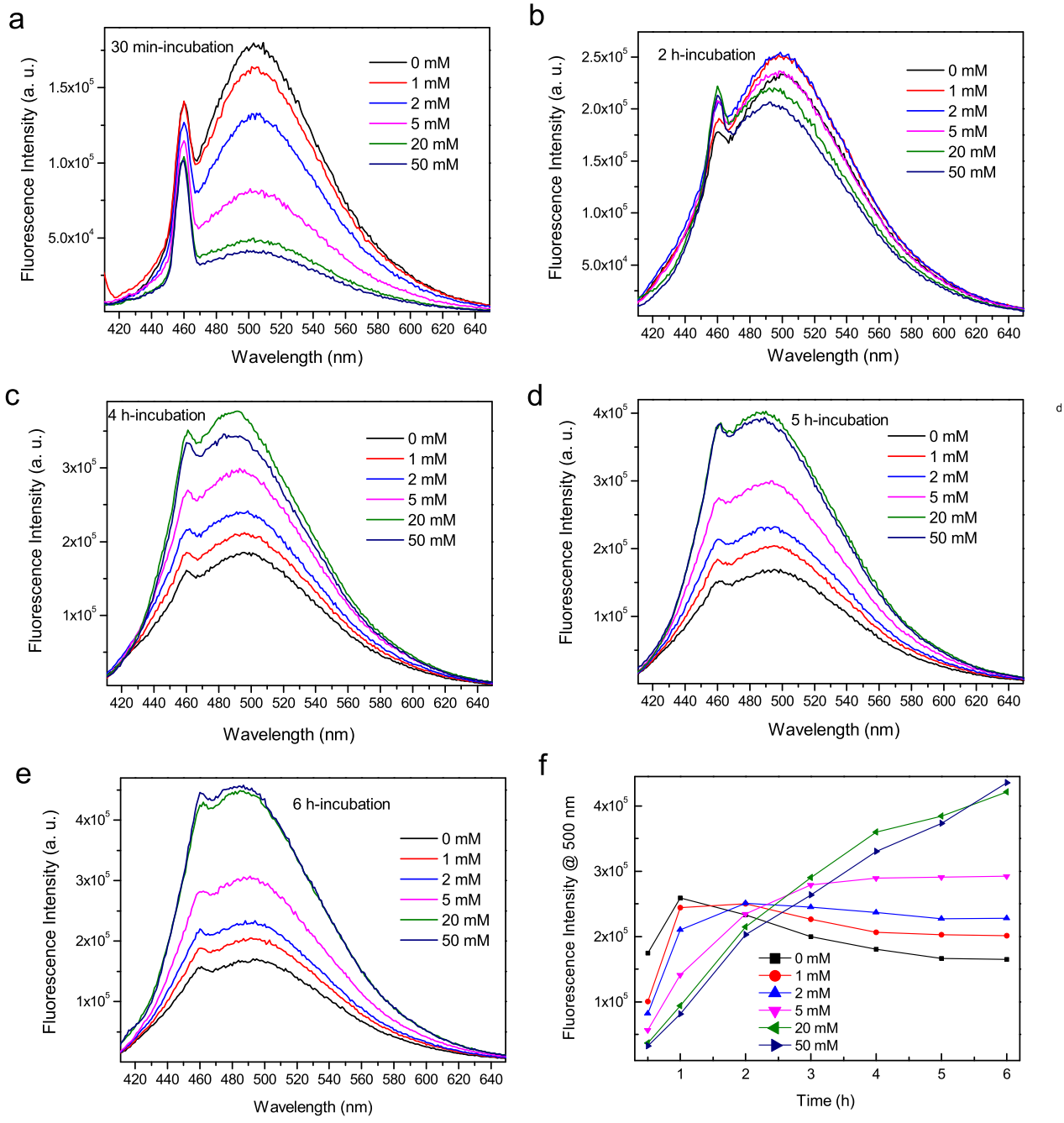


Figure 5.9: a) Fluorescence spectra of PDA after incubation with glucose with concentration ranging from 1 mM to 50 mM in bulk glucose/glucose oxidase (GOx) solutions for (a) 30 min, (b) 2 h, (c) 4 h, (d) 5 h and (e) 6 h (f) Time-dependence of fluorescence intensities at 500 nm plotted with data in a, b, c, d and e.

In summary, a simple detection platform was fabricated for glucose based on polydopamine fluorescence by using small volume droplets on superhydrophilic-superhydrophobic patterned surfaces. Glucose can be sensitively anayzed in evaporating droplets due to enrichment-induced rapid reactions. Polydopamine can eliminate the use of additional enzyme for $H_2O_2$ analysis.

# Chapter 6

# Droplet-based DNA Detection on Superhydrophilic-Patterned Surfaces

Numerous DNA biosensors have been developed in the last decade. To achieve the ultrasensitive detection of DNA molecules, signal amplification strategies were used including enzyme-catalysis and polymerase chain reaction [99]. However, enrichment is necessary for low concentration small volumes DNA samples. Superhydrophilic-patterned superhydrophobic surfaces were used for detection of trace amount biomolecules based-on enrichment-induced enhancement of SERS signals [98]. In this thesis, wetted patterns were functionalized with single stranded DNA and fluorescence-based DNA sensing was performed in evaporating micro droplets. Hybridization of target and probe DNA strands inside droplets resulted with higher fluorescence intensities compared to that in mL-scale bulk solution where no enrichment occurred. Fluorescence of hybridized DNA with concentration as low as 200 fM was detected thanks to the enrichment effect of patterned surfaces.

## 6.1 Experimental Section

### 6.1.1 Materials

Sodium hydroxide, ethanol and hydrochloric acid were purchased from Merck. Phosphate buffered saline (PBS) tablets, (3-Glycidoxypropyl) trimethoxy silane (GOPTS), sodium carbonate and bovine serum albumin (BSA) were purchased from Sigma-Aldrich. Molecular biology grade (MB grade) water was purchased from Fisher Scientific. All chemicals were used as received. Amino-modified, Cy5-tagged and Cy3-tagged single stranded DNA (ss-DNA) sequences were purchased from Sentegen Biotech (Ankara, Turkey). Sequences were as follows:

-Probe DNA: 5'-C6-Amino-TTGGAACATTC-Cy5-3' (fluorescence-tagged)

-Target DNA: 5'-Cy3-GAATGTTCCAA-3'

-Non-complementary DNA: 5'-Cy3-TGCCGCTGCAC-3'

### 6.1.2 Preparation of buffer solutions

100 mM PBS buffer was prepared by dissolving 10 PBS tablets in 200 mL of deionized water and solution pH was adjusted to 7.4 using 1 M sodium hydroxide solution. 100 mM sodium carbonate buffer was prepared and its pH was adjusted to 9.0 using 2 M hydrochloric acid.

### 6.1.3 DNA assay

Patterned surfaces were dipped into ethanol solution containing 2% (v/v) GOPTS and incubated at 37 °C overnight. Then, surfaces were washed with ethanol for several times followed by drying at 120 °C for 1 h. 4 $\mu$L portions of 1 $\mu$M Cy5-tagged probe DNA in sodium carbonate buffer solutions (pH=9.0) were drop-cast

onto super-wetted spots. After incubation at 37 °C for 4 h in a closed chamber humidified around 80%, surfaces were washed with PBS solutions (pH=7.4) to remove unbound DNA strands. Surfaces were then washed with PBS buffer followed by washing with 1% BSA-PBS solution and MB grade water, respectively. 4 $\mu$L of target DNA (200 fM, 20 pM and 200 pM) in PBS solutions were drop-cast onto probe-bound spots. Micro droplets were left to incubate in dark at 37 °C for 2 h in a closed chamber with 40% humidity. Surfaces were then washed with PBS (pH=7.4) and MB grade water, respectively and dried with nitrogen blow.

### 6.1.4 DNA detection experiments

Fluorescent images of droplet-based DNA assay were taken with confocal microscope (Model LSM 510, Zeiss, Germany) using 10X objective. Helium lasers at 543 nm and 633 nm were used for excitation. Emissions at around 570 nm and 650 nm were collected for Cy3 and Cy5, respectively.

## 6.2 Results and Discussion

A droplet-based DNA detection was developed to demonstrate the adaptability of patterned surfaces for DNA sensing. First, single stranded DNA molecules were covalently attached to wetted patterns as probe DNA using silane-chemistry. Briefly, wetted patterns were first epoxylated with GOPTS and then amine-ended DNA molecules were anchored to epoxy groups in sodium carbonate buffer with a pH of 9 (Figure 6.1).

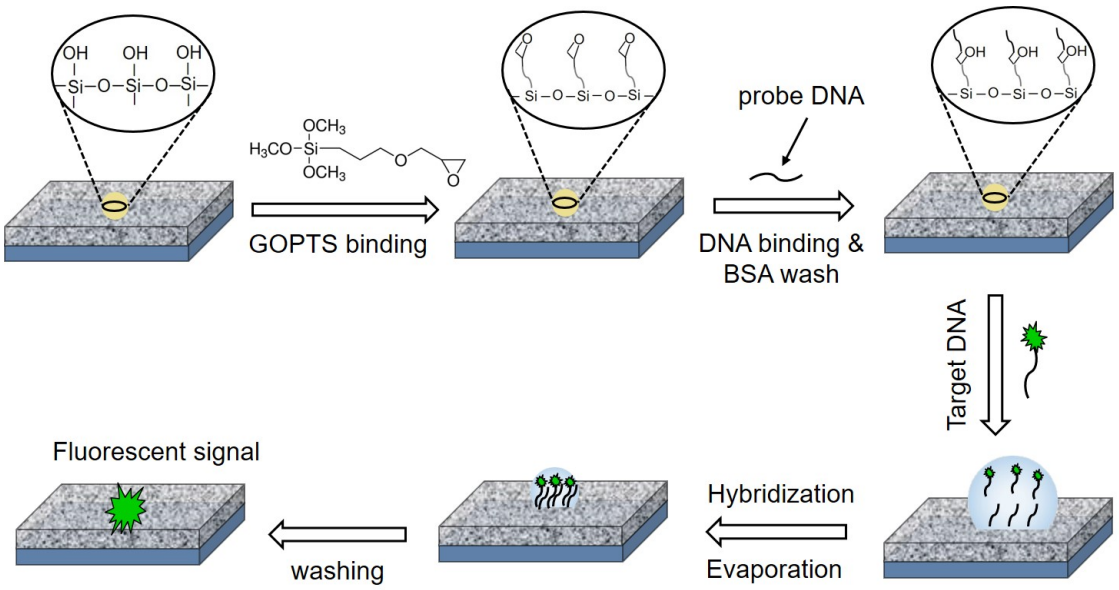


Figure 6.1: Schematic representation of epoxy-silane binding onto UV/Ozone-treated patterns followed by attachment of probe DNA, droplet-based hybridization of fluorescence-tagged target DNA, evaporation-induced analyte enrichment and fluorescence enhancement.

Surfaces were washed with BSA solution to remove the unbound DNA molecules. Binding of GOPTS and DNA to UV/Ozone-treated patterns was analyzed with X-ray photoelectron spectroscopy. C1s spectrum of UV/Ozone-treated areas showed the decomposition of $CH_3$ groups (Figure 6.2a-b). Peaks at 286.7 eV and 287.7 eV confirmed epoxy-silane binding (Figure 6.2c) [122].

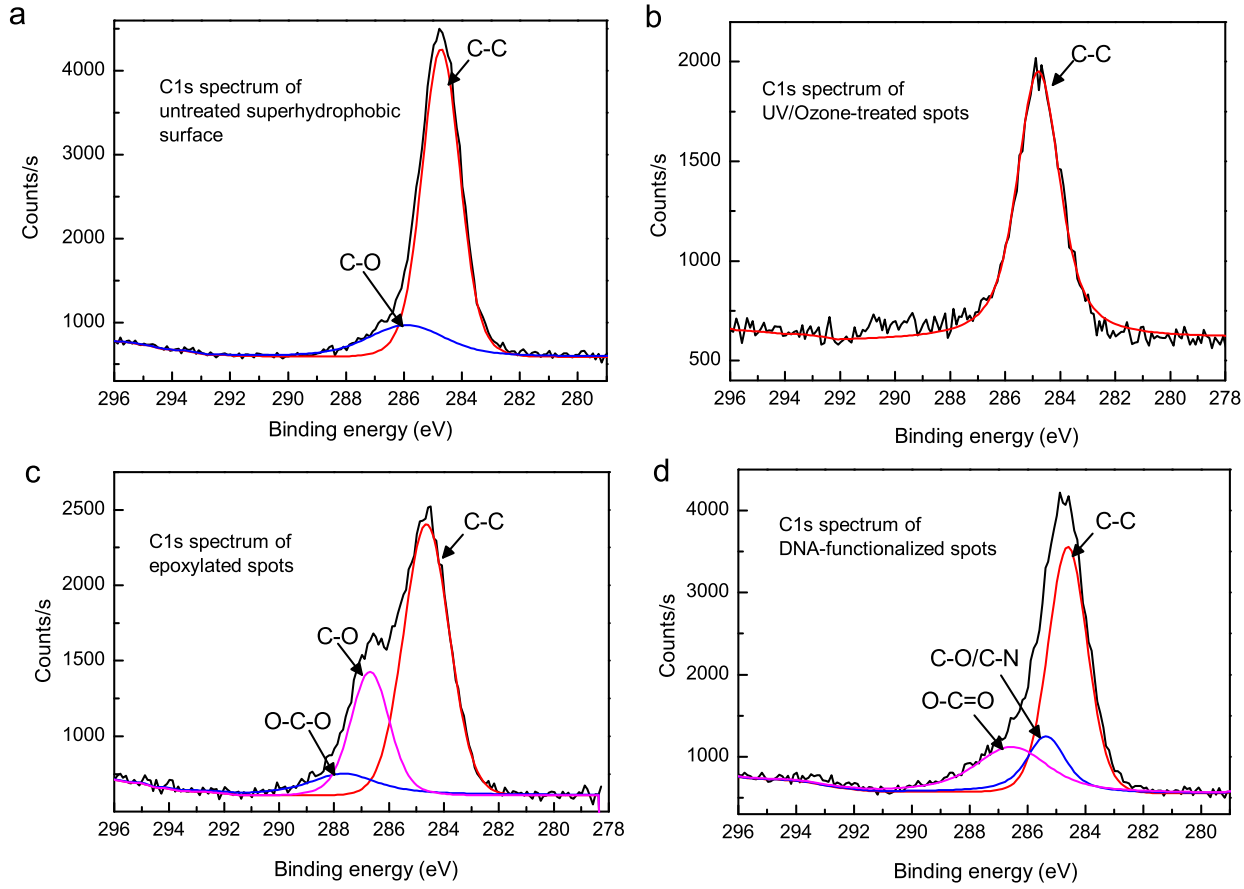


Figure 6.2: a) C1s XPS spectrum of untreated superhydrophobic surface. b) C1s XPS spectrum of UV/ozone-treated patterns. c) C1s XPS spectrum of of epoxylated pattern. d) C1s XPS spectrum of DNA-functionalized pattern.

Binding of probe DNA was also monitored with confocal microscopy using Cy5 tagging. Red emission of Cy5 collected from porous organically modified silica (ormosil) network showed that probe DNA uniformly bonded all over the epoxy-functionalized silica nanoparticles on wetted pattern (Figure 6.3a). 4 $\mu$L of droplets including Cy3-tagged 200 fM, 20 pM and 200 pM target DNA were added to probe-bound patterns and left to incubate while evaporating in the meantime. After washing with BSA and PBS buffer solutions, emission intensities were analyzed with confocal microscopy. Figure 6.3b shows fluorescence signal collected after hybridization of 20 pM target DNA.

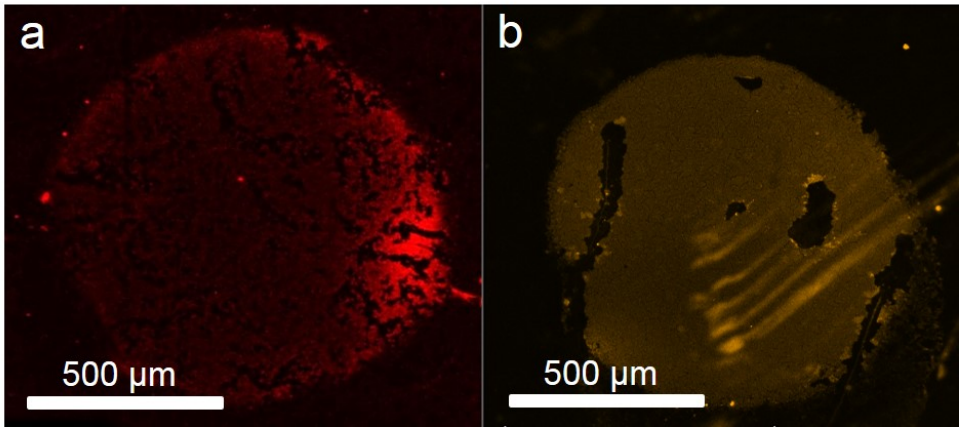


Figure 6.3: a) Confocal image of wetted pattern after the attachment of Cy5-tagged probe DNA. b) Confocal image of wetted pattern after hybridization of probe DNA with 20 pM Cy3-tagged target DNA in 4 $\mu$L of evaporating droplet.

Fluorescence signals of confocal images were converted to numerical intensity values. Hybridization signal for non-complementary DNA was at the same level with that in buffer solution and fluorescence increased with target DNA concentration increasing from 200 fM to 200 pM (Figure 6.4).

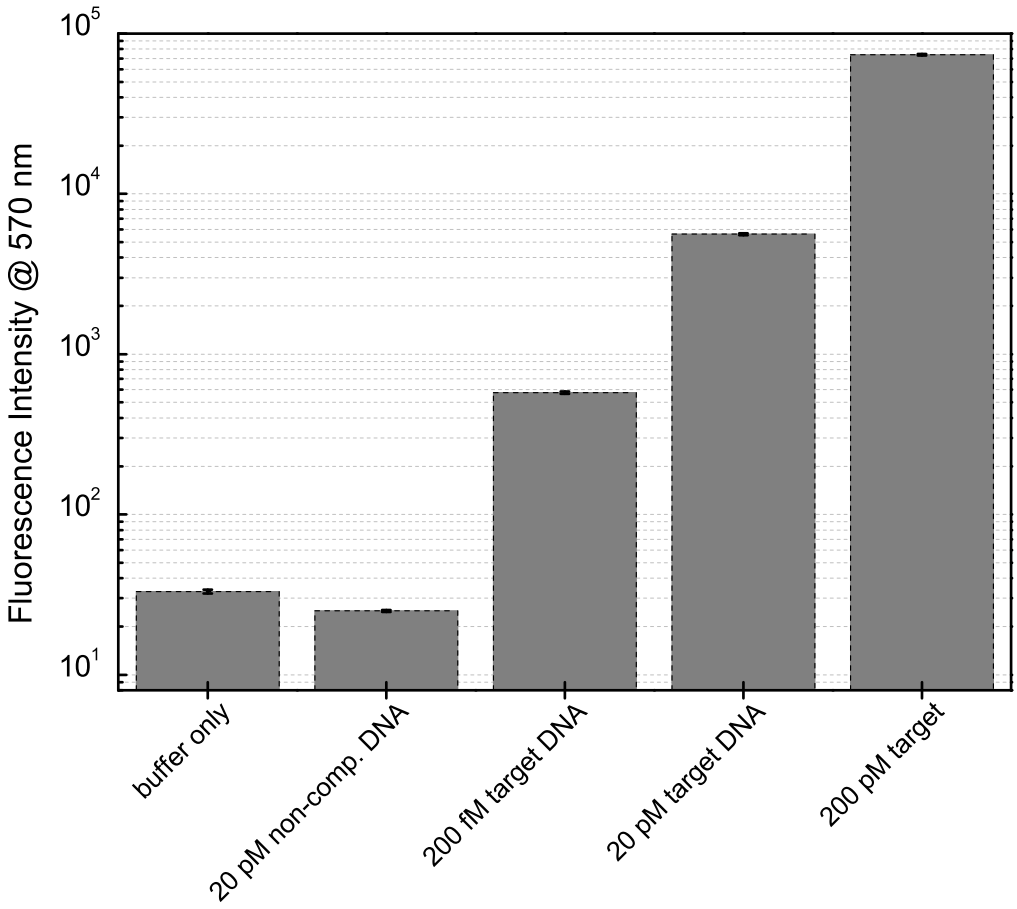


Figure 6.4: Fluorescence intensities calculated from confocal images of patterns incubated with droplets containing buffer without DNA; 20 pM non-complementary DNA; 20 pM, 200 fM and 200 pM target DNA. Intensities are average of three repeated hybridization.

In addition, hybridization was performed in mL-scale bulk solution. A surface with probe DNA anchored on 0.9 mm-pattern was immersed in 2 mL of 20 pM target DNA solution and left to incubate. After washing, pattern was analyzed with confocal imaging. Fluorescence signal obtained in droplet-based assay was higher than that in solution-based assay by two orders of magnitude (Figure 6.5).

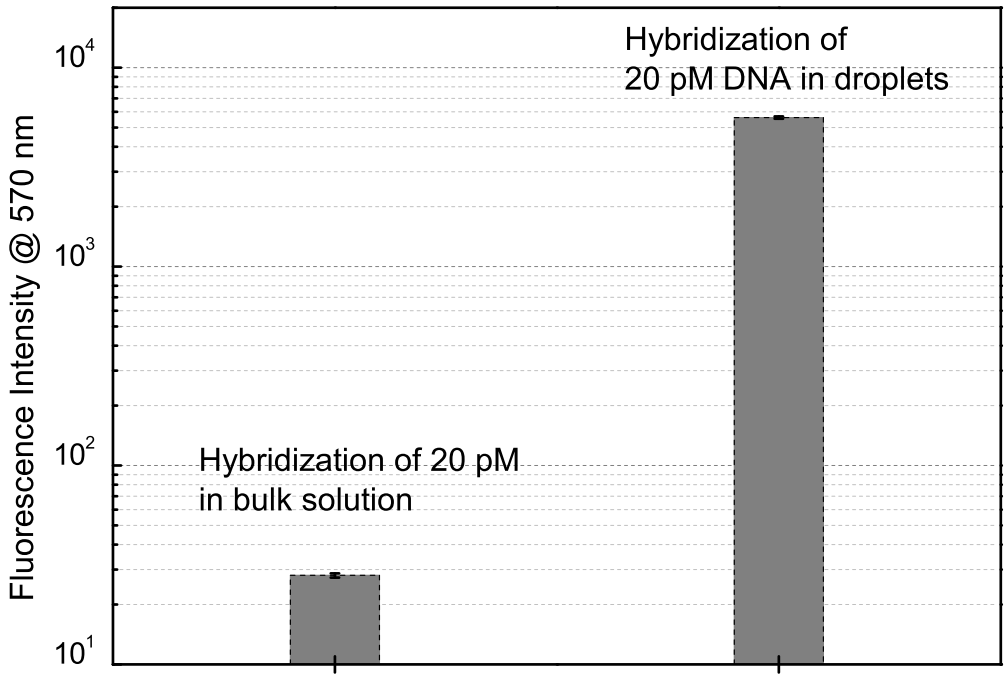


Figure 6.5: Comparison of fluorescence intensities of 20 pM target DNA hybridized in evaporating droplet with 20 pM target DNA hybridized in 2 mL bulk solution where no enrichment occured. Intensities were average of three repeated hybridization.

In summary, wetted patterns were functionalized with DNA strands and were used for droplet-based DNA analysis using very low sample volumes.

# Chapter 7

# Conclusions

In conclusion, this thesis introduces novel silica nanomaterials designed and synthesized for sensitive detection of toxic material and biological molecule sensing. Sensor materials have been prepared in the form of colloidal aqueous solutions or in the form of porous thin films.

First, a facile and low-cost method was developed to prepare pyrene confined mesostructured silica nanoparticles (pMSNs) for sensitive detection of TNT and dopamine in water. Pyrene was encapsulated in mesostructured nanoparticles through hydrophobic-hydrophobic interactions between cetylrimethylammonium (CTA) micelles and pyrene. Spherical or rod-shaped organic/inorganic hybrid nanoparticles had fairly uniform size distribution and good colloidal stability in water. Bright and visible pyrene excimer emission was observed for pMSNs which was stable for at least six months. Excimer emission of pMSNs exhibited rapid quenching against analyte molecules. Detection limits for TNT and dopamine were calculated as 12 nM and 300 nM, respectively. Furthermore, quenching of the excimer emission was visually observed under UV-light suggesting naked-eye detection at submicromolar level. Pyrene confined mesostructured silica nanoparticles hold a significant potential for rapid and reliable detection with their simple synthesis and sensitivity.

Secondly, superhydrophilic patterning on superhydrophobic organically modified silica (ormosil) surfaces was demonstrated. Ormosil is an intrinsically superhydrophobic inorganic-organic hybrid structure and can be applied as functional nanoporous coating on different substrates including glass, silicon and polymer. UV/ozone (UV/O) treatment on selected areas of ormosil surface leads to the formation of very stable superhydrophilic patterns without changing surface morphology. Arrays of droplets can be formed in desired size and shape on both flexible and rigid materials. Super-wetted patterns can capture any water-soluble materials which can be used for high-throughput molecular screening.

Thirdly, a simple detection platform was fabricated for glucose and DNA assays by using superhydrophilic-superhydrophobic patterned surfaces. A simple UV/O-based chemical treatment was used to generate wetted patterns on superhydrophobic coatings produced via sol-gel method. Very small volume aqueous droplets can be confined on wetted patterns. Analytes dissolved in droplets can be enriched upon evaporation of micro droplets which are confined on wetted patterns. Polydopamine (PDA) was used as a single fluorescent probe for glucose, for the first time in this study, by benefitting from hydrogen peroxide ($H_2O_2$)-dependent fluorescent enhancement of PDA. A glucose assay with reduced response time and increased sensitivity was obtained due to enrichment-induced increase of reactions rates. Contrary to droplet-based assay, fluorescence enhancement was very slow in bulk solutions. Glucose detection with concentration ranging from 1 mM to 50 mM was shown using bright PDA fluorescence which can also be observed by naked-eye. PDA with its biocompatibility and promising response curve shows potential for replacing the horseradish peroxidase/chromogen indicators in glucose sensors especially for wearable and implantable sensors. Furthermore, wetted patterns were functionalized with DNA strands and were used for droplet-based DNA analysis using very low sample volumes. Target DNA with concentration as low as 200 fM can be detected by means of enrichment effect. We believe that the presented patterned surfaces with high sensitivity and simple production have potential for a wide range of biochemical analysis.

As a future work, protein-protein interactions and cell growth on patterned surfaces will be investigated.

# Bibliography


[1] A. P. F. Turner, "Biosensors: sense and sensibility," *Chem. Soc. Rev.*, vol. 42, pp. 3184–3196, 2013.

[2] J. Kirsch, C. Siltanen, Q. Zhou, A. Revzin, and A. Simonian, "Biosensor technology: recent advances in threat agent detection and medicine," *Chem. Soc. Rev.*, vol. 42, pp. 8733–8768, 2013.

[3] D. Grieshaber, R. MacKenzie, J. Vörös, and E. Reimhult, "Electrochemical biosensors - sensor principles and architectures," *Sensors*, vol. 8, no. 3, pp. 1400–1458, 2008.

[4] T. Asefa, C. T. Duncan, and K. K. Sharma, "Recent advances in nanostructured chemosensors and biosensors," *Analyst*, vol. 134, pp. 1980–1990, 2009.

[5] L. Shang, S. Dong, and G. U. Nienhaus, "Ultra-small fluorescent metal nanoclusters: Synthesis and biological applications," *Nano Today*, vol. 6, no. 4, pp. 401–418, 2011.

[6] J. Wu, W. Liu, J. Ge, H. Zhang, and P. Wang, "New sensing mechanisms for design of fluorescent chemosensors emerging in recent years," *Chem. Soc. Rev.*, vol. 40, pp. 3483–3495, 2011.

[7] L. Basabe-Desmonts, D. N. Reinhoudt, and M. Crego-Calama, "Design of fluorescent materials for chemical sensing," *Chem. Soc. Rev.*, vol. 36, pp. 993–1017, 2007.

[8] O. S. Wolfbeis, "Materials for fluorescence-based optical chemical sensors," *J. Mater. Chem.*, vol. 15, pp. 2657–2669, 2005.

[9] V. Biju, "Chemical modifications and bioconjugate reactions of nanomaterials for sensing, imaging, drug delivery and therapy," *Chem. Soc. Rev.*, vol. 43, pp. 744–764, 2014.

[10] M. E. Germain and M. J. Knapp, "Optical explosives detection: from color changes to fluorescence turn-on," *Chem. Soc. Rev.*, vol. 38, pp. 2543–2555, 2009.

[11] Y. Salinas, R. Martinez-Manez, M. D. Marcos, F. Sancenon, A. M. Costero, M. Parra, and S. Gil, "Optical chemosensors and reagents to detect explosives," *Chem. Soc. Rev.*, vol. 41, pp. 1261–1296, 2012.

[12] S. Singh, "Sensors—an effective approach for the detection of explosives," *Journal of Hazardous Materials*, vol. 144, no. 1, pp. 15–28, 2007.

[13] J. S. Caygill, F. Davis, and S. P. Higson, "Current trends in explosive detection techniques," *Talanta*, vol. 88, pp. 14–29, 2012.

[14] D. S. Moore, "Instrumentation for trace detection of high explosives," *Review of Scientific Instruments*, vol. 75, no. 8, pp. 2499–2512, 2004.

[15] S. J. Toal and W. C. Trogler, "Polymer sensors for nitroaromatic explosives detection," *J. Mater. Chem.*, vol. 16, pp. 2871–2883, 2006.

[16] K. Zhang, H. Zhou, Q. Mei, S. Wang, G. Guan, R. Liu, J. Zhang, and Z. Zhang, "Instant visual detection of trinitrotoluene particulates on various surfaces by ratiometric fluorescence of dual-emission quantum dots hybrid," *Journal of the American Chemical Society*, vol. 133, no. 22, pp. 8424–8427, 2011. PMID: 21563794.

[17] R. Freeman, T. Finder, L. Bahshi, R. Gill, and I. Willner, "Functionalized CdSe/ZnS QDs for the detection of nitroaromatic or RDX explosives," *Advanced Materials*, vol. 24, no. 48, pp. 6416–6421, 2012.

[18] S. Xu, H. Lu, J. Li, X. Song, A. Wang, L. Chen, and S. Han, "Dummy molecularly imprinted polymers-capped CdTe quantum dots for the fluorescent sensing of 2,4,6-trinitrotoluene," *ACS Applied Materials & Interfaces*, vol. 5, no. 16, pp. 8146–8154, 2013. PMID: 23876063.

[19] D. Li, J. Liu, R. T. K. Kwok, Z. Liang, B. Z. Tang, and J. Yu, "Supersensitive detection of explosives by recyclable AIE luminogen-functionalized mesoporous materials," *Chem. Commun.*, vol. 48, pp. 7167–7169, 2012.

[20] A. Rana and P. K. Panda, "Fluorescent turn-off based sensing of nitrated explosives using porphyrins and their $Zn^{2+}$ derivatives," *RSC Adv.*, vol. 2, pp. 12164–12168, 2012.

[21] S. Shanmugaraju, S. A. Joshi, and P. S. Mukherjee, "Fluorescence and visual sensing of nitroaromatic explosives using electron rich discrete fluorophores," *J. Mater. Chem.*, vol. 21, pp. 9130–9138, 2011.

[22] H. Li, Y. Zhu, J. Zhang, Z. Chi, L. Chen, and C.-Y. Su, "Luminescent metal-organic gels with tetraphenylethylene moieties: porosity and aggregation-induced emission," *RSC Adv.*, vol. 3, pp. 16340–16344, 2013.

[23] B. Gole, A. K. Bar, and P. S. Mukherjee, "Fluorescent metal-organic framework for selective sensing of nitroaromatic explosives," *Chem. Commun.*, vol. 47, pp. 12137–12139, 2011.

[24] Y.-N. Gong, L. Jiang, and T.-B. Lu, "A highly stable dynamic fluorescent metal-organic framework for selective sensing of nitroaromatic explosives," *Chem. Commun.*, vol. 49, pp. 11113–11115, 2013.

[25] D. T. McQuade, A. E. Pullen, and T. M. Swager, "Conjugated polymer-based chemical sensors," *Chemical Reviews*, vol. 100, no. 7, pp. 2537–2574, 2000. PMID: 11749295.

[26] L. Feng, H. Li, Y. Qu, and C. Lu, "Detection of TNT based on conjugated polymer encapsulated in mesoporous silica nanoparticles through FRET," *Chem. Commun.*, vol. 48, pp. 4633–4635, 2012.

[27] Y. Z. Liao, V. Strong, Y. Wang, X.-G. Li, X. Wang, and R. B. Kaner, "Oligotriphenylene nanofiber sensors for detection of nitro-based explosives," *Advanced Functional Materials*, vol. 22, no. 4, pp. 726–735, 2012.

[28] T. M. Figueira-Duarte and K. Mullen, "Pyrene-based materials for organic electronics," *Chemical Reviews*, vol. 111, no. 11, pp. 7260–7314, 2011. PMID: 21740071.

[29] Y. Wang, A. La, Y. Ding, Y. Liu, and Y. Lei, "Novel signal-amplifying fluorescent nanofibers for naked-eye-based ultrasensitive detection of buried explosives and explosive vapors," *Advanced Functional Materials*, vol. 22, no. 17, pp. 3547–3555, 2012.

[30] G. B. Demirel, B. Daglar, and M. Bayindir, "Extremely fast and highly selective detection of nitroaromatic explosive vapours using fluorescent polymer thin films," *Chem. Commun.*, vol. 49, pp. 6140–6142, 2013.

[31] H. Du, G. He, T. Liu, L. Ding, and Y. Fang, "Preparation of pyrene-functionalized fluorescent film with a benzene ring in spacer and sensitive detection to picric acid in aqueous phase," *Journal of Photochemistry and Photobiology A: Chemistry*, vol. 217, no. 2, pp. 356 – 362, 2011.

[32] T. Liu, L. Ding, K. Zhao, W. Wang, and Y. Fang, "Single-layer assembly of pyrene end-capped terthiophene and its sensing performances to nitroaromatic explosives," *J. Mater. Chem.*, vol. 22, pp. 1069–1077, 2012.

[33] G. He, N. Yan, J. Yang, H. Wang, L. Ding, S. Yin, and Y. Fang, "Pyrene-containing conjugated polymer-based fluorescent films for highly sensitive and selective sensing of TNT in aqueous medium," *Macromolecules*, vol. 44, no. 12, pp. 4759–4766, 2011.

[34] Y. Wang, A. La, C. Bruckner, and Y. Lei, "FRET- and PET-based sensing in a single material: expanding the dynamic range of an ultra-sensitive nitroaromatic explosives assay," *Chem. Commun.*, vol. 48, pp. 9903–9905, 2012.

[35] A. Vu, J. Phillips, P. Buhlmann, and A. Stein, "Quenching performance of surfactant-containing and surfactant-free fluorophore-doped mesoporous silica films for nitroaromatic compound detection," *Chemistry of Materials*, vol. 25, no. 5, pp. 711–722, 2013.

[36] K. Sarkar, Y. Salinas, I. Campos, R. Martínez-Máñez, M. D. Marcos, F. Sancenón, and P. Amorós, "Organic–inorganic hybrid mesoporous materials as regenerable sensing systems for the recognition of nitroaromatic explosives," *ChemPlusChem*, vol. 78, no. 7, pp. 684–694, 2013.

[37] W. Chen, N. B. Zuckerman, J. P. Konopelski, and S. Chen, "Pyrene-functionalized ruthenium nanoparticles as effective chemosensors for nitroaromatic derivatives," *Analytical Chemistry*, vol. 82, no. 2, pp. 461–465, 2010. PMID: 20000846.

[38] E.-B. Cho, D. O. Volkov, and I. Sokolov, "Ultrabright fluorescent silica mesoporous silica nanoparticles: Control of particle size and dye loading," *Advanced Functional Materials*, vol. 21, no. 16, pp. 3129–3135, 2011.

[39] S. Palantavida, R. Tang, G. P. Sudlow, W. J. Akers, S. Achilefu, and I. Sokolov, "Ultrabright NIR fluorescent mesoporous silica nanoparticles," *J. Mater. Chem. B*, vol. 2, pp. 3107–3114, 2014.

[40] J. S. Beck, J. C. Vartuli, W. J. Roth, M. E. Leonowicz, C. T. Kresge, K. D. Schmitt, C. T. W. Chu, D. H. Olson, E. W. Sheppard, S. B. McCullen, J. B. Higgins, and J. L. Schlenker, "A new family of mesoporous molecular sieves prepared with liquid crystal templates," *Journal of the American Chemical Society*, vol. 114, no. 27, pp. 10834–10843, 1992.

[41] Q. Cai, Z.-S. Luo, W.-Q. Pang, Y.-W. Fan, X.-H. Chen, and F.-Z. Cui, "Dilute solution routes to various controllable morphologies of MCM-41 silica with a basic medium," *Chemistry of Materials*, vol. 13, no. 2, pp. 258–263, 2001.

[42] M. Liong, J. Lu, M. Kovochich, T. Xia, S. G. Ruehm, A. E. Nel, F. Tamanoi, and J. I. Zink, "Multifunctional inorganic nanoparticles for imaging, targeting, and drug delivery," *ACS Nano*, vol. 2, no. 5, pp. 889–896, 2008. PMID: 19206485.

[43] A. Yildirim, H. Budunoglu, B. Daglar, H. Deniz, and M. Bayindir, "One-pot preparation of fluorinated mesoporous silica nanoparticles for liquid marble formation and superhydrophobic surfaces," *ACS Applied Materials & Interfaces*, vol. 3, no. 6, pp. 1804–1808, 2011. PMID: 21574636.

[44] K. Suzuki, K. Ikari, and H. Imai, "Synthesis of silica nanoparticles having a well-ordered mesostructure using a double surfactant system," *Journal of the American Chemical Society*, vol. 126, no. 2, pp. 462–463, 2004. PMID: 14719932.

[45] S. Febvay, D. M. Marini, A. M. Belcher, and D. E. Clapham, "Targeted cytosolic delivery of cell-impermeable compounds by nanoparticle-mediated, light-triggered endosome disruption," *Nano Letters*, vol. 10, no. 6, pp. 2211–2219, 2010. PMID: 20446663.

[46] F. M. Winnik, "Photophysics of preassociated pyrenes in aqueous polymer solutions and in other organized media," *Chemical Reviews*, vol. 93, no. 2, pp. 587–614, 1993.

[47] J. B. Birks, "Excimers," *Reports on Progress in Physics*, vol. 38, no. 8, p. 903, 1975.

[48] J.-S. Yang and T. M. Swager, "Fluorescent porous polymer films as TNT chemosensors:? electronic and structural effects," *Journal of the American Chemical Society*, vol. 120, no. 46, pp. 11864–11873, 1998.

[49] A. Sawa and S. H. Snyder, "Schizophrenia: Diverse approaches to a complex disease," *Science*, vol. 296, no. 5568, pp. 692–695, 2002.

[50] Y. Lin, C. Chen, C. Wang, F. Pu, J. Ren, and X. Qu, "Silver nanoprobe for sensitive and selective colorimetric detection of dopaminevia robust ag-catechol interaction," *Chem. Commun.*, vol. 47, pp. 1181–1183, 2011.

[51] R. M. Wightman, L. J. May, and A. C. Michael, "Detection of dopamine dynamics in the brain," *Analytical Chemistry*, vol. 60, no. 13, pp. 769A–779A, 1988. PMID: 3063135.

[52] T. Qian, S. Wu, and J. Shen, "Facilely prepared polypyrrole-reduced graphite oxide core-shell microspheres with high dispersibility for electrochemical detection of dopamine," *Chem. Commun.*, vol. 49, pp. 4610–4612, 2013.

[53] R. Ban, E. S. Abdel-Halim, J. Zhang, and J.-J. Zhu, "[small beta]-cyclodextrin functionalised gold nanoclusters as luminescence probes for the ultrasensitive detection of dopamine," *Analyst*, vol. 140, pp. 1046–1053, 2015.

[54] X. Zhou, P. Ma, A. Wang, C. Yu, T. Qian, S. Wu, and J. Shen, "Dopamine fluorescent sensors based on polypyrrole/graphene quantum dots core/shell hybrids," *Biosensors and Bioelectronics*, vol. 64, pp. 404 – 410, 2015.

[55] S. Nishimoto and B. Bhushan, "Bioinspired self-cleaning surfaces with superhydrophobicity, superoleophobicity, and superhydrophilicity," *RSC Adv.*, vol. 3, pp. 671–690, 2013.

[56] L. Zhai, M. C. Berg, F. Cebeci, Y. Kim, J. M. Milwid, M. F. Rubner, and R. E. Cohen, "Patterned superhydrophobic surfaces: Toward a synthetic mimic of the namib desert beetle," *Nano Letters*, vol. 6, no. 6, pp. 1213–1217, 2006. PMID: 16771582.

[57] R. P. Garrod, L. G. Harris, W. C. E. Schofield, J. McGettrick, L. J. Ward, D. O. H. Teare, and J. P. S. Badyal, "Mimicking a stenocara beetle's back for microcondensation using plasmachemical patterned superhydrophobic-superhydrophilic surfaces," *Langmuir*, vol. 23, no. 2, pp. 689–693, 2007. PMID: 17209621.

[58] H. Bai, L. Wang, J. Ju, R. Sun, Y. Zheng, and L. Jiang, "Efficient water collection on integrative bioinspired surfaces with star-shaped wettability patterns," *Advanced Materials*, vol. 26, no. 29, pp. 5025–5030, 2014.

[59] L. Zhang, J. Wu, M. N. Hedhili, X. Yang, and P. Wang, "Inkjet printing for direct micropatterning of a superhydrophobic surface: toward biomimetic fog harvesting surfaces," *J. Mater. Chem. A*, vol. 3, pp. 2844–2852, 2015.

[60] N. M. Oliveira, A. I. Neto, W. Song, and J. F. Mano, "Two-dimensional open microfluidic devices by tuning the wettability on patterned superhydrophobic polymeric surface," *Applied Physics Express*, vol. 3, no. 8, p. 085205, 2010.

[61] K. Choi, A. H. Ng, R. Fobel, and A. R. Wheeler, "Digital microfluidics," *Annual Review of Analytical Chemistry*, vol. 5, no. 1, pp. 413–440, 2012. PMID: 22524226.

[62] P. Lam, K. J. Wynne, and G. E. Wnek, "Surface-tension-confined microfluidics," *Langmuir*, vol. 18, no. 3, pp. 948–951, 2002.

[63] I. You, N. Yun, and H. Lee, "Surface-tension-confined microfluidics and their applications," *ChemPhysChem*, vol. 14, no. 3, pp. 471–481, 2013.

[64] S. Xing, J. Jiang, and T. Pan, "Interfacial microfluidic transport on micropatterned superhydrophobic textile," *Lab Chip*, vol. 13, pp. 1937–1947, 2013.

[65] J. Songok, M. Tuominen, H. Teisala, J. Haapanen, J. Makela, J. Kuusipalo, and M. Toivakka, "Paper-based microfluidics: Fabrication technique and dynamics of capillary-driven surface flow," *ACS Applied Materials & Interfaces*, vol. 6, no. 22, pp. 20060–20066, 2014. PMID: 25336235.

[66] E. Ueda and P. A. Levkin, "Emerging applications of superhydrophilic-superhydrophobic micropatterns," *Advanced Materials*, vol. 25, no. 9, pp. 1234–1247, 2013.

[67] E. Gogolides, K. Ellinas, and A. Tserepi, "Hierarchical micro and nano structured, hydrophilic, superhydrophobic and superoleophobic surfaces incorporated in microfluidics, microarrays and lab-on-chip microsystems," *Microelectronic Engineering*, vol. 132, pp. 135–155, 2015. Micro and Nanofabrication Breakthroughs for Electronics, MEMS and Life Sciences.

[68] A. I. Neto, C. A. Custodio, W. Song, and J. F. Mano, "High-throughput evaluation of interactions between biomaterials, proteins and cells using patterned superhydrophobic substrates," *Soft Matter*, vol. 7, pp. 4147–4151, 2011.

[69] E. Ueda, F. L. Geyer, V. Nedashkivska, and P. A. Levkin, "Droplet microarray: facile formation of arrays of microdroplets and hydrogel micropads for cell screening applications," *Lab Chip*, vol. 12, pp. 5218–5224, 2012.

[70] A. I. Neto, C. R. Correia, C. A. Custódio, and J. F. Mano, "Biomimetic miniaturized platform able to sustain arrays of liquid droplets for high-throughput combinatorial tests," *Advanced Functional Materials*, vol. 24, no. 32, pp. 5096–5103, 2014.

[71] F. L. Geyer, E. Ueda, U. Liebel, N. Grau, and P. A. Levkin, "Superhydrophobic–superhydrophilic micropatterning: Towards genome-on-a-chip cell microarrays," *Angewandte Chemie International Edition*, vol. 50, no. 36, pp. 8424–8427, 2011.

[72] H. S. Lim, J. T. Han, D. Kwak, M. Jin, and K. Cho, "Photoreversibly switchable superhydrophobic surface with erasable and rewritable pattern," *Journal of the American Chemical Society*, vol. 128, no. 45, pp. 14458–14459, 2006. PMID: 17090019.

[73] S. J. Pastine, D. Okawa, B. Kessler, M. Rolandi, M. Llorente, A. Zettl, and J. M. J. Frechet, "A facile and patternable method for the surface modification of carbon nanotube forests using perfluoroarylazides," *Journal of the American Chemical Society*, vol. 130, no. 13, pp. 4238–4239, 2008. PMID: 18331043.

[74] D. Zahner, J. Abagat, F. Svec, J. M. J. Fréchet, and P. A. Levkin, "A facile approach to superhydrophilic–superhydrophobic patterns in porous polymer films," *Advanced Materials*, vol. 23, no. 27, pp. 3030–3034, 2011.

[75] W. Feng, L. Li, E. Ueda, J. Li, S. Heißler, A. Welle, O. Trapp, and P. A. Levkin, "Surface patterning via thiol-yne click chemistry: An extremely fast and versatile approach to superhydrophilic-superhydrophobic

micropatterns," *Advanced Materials Interfaces*, vol. 1, no. 7, p. 1400269, 2014.

[76] X. Li, J. Tian, T. Nguyen, and W. Shen, "Paper-based microfluidic devices by plasma treatment," *Analytical Chemistry*, vol. 80, no. 23, pp. 9131–9134, 2008. PMID: 19551982.

[77] V. Jokinen, L. Sainiemi, and S. Franssila, "Complex droplets on chemically modified silicon nanograss," *Advanced Materials*, vol. 20, no. 18, pp. 3453–3456, 2008.

[78] S. P. R. Kobaku, A. K. Kota, D. H. Lee, J. M. Mabry, and A. Tuteja, "Patterned superomniphobic–superomniphilic surfaces: Templates for site-selective self-assembly," *Angewandte Chemie International Edition*, vol. 51, no. 40, pp. 10109–10113, 2012.

[79] J. S. Li, E. Ueda, A. Nallapaneni, L. X. Li, and P. A. Levkin, "Printable superhydrophilic superhydrophobic micropatterns based on supported lipid layers," *Langmuir*, vol. 28, no. 22, pp. 8286–8291, 2012. PMID: 22594681.

[80] U. Manna, A. H. Broderick, and D. M. Lynn, "Chemical patterning and physical refinement of reactive superhydrophobic surfaces," *Advanced Materials*, vol. 24, no. 31, pp. 4291–4295, 2012.

[81] D. Tian, Y. Song, and L. Jiang, "Patterning of controllable surface wettability for printing techniques," *Chem. Soc. Rev.*, vol. 42, pp. 5184–5209, 2013.

[82] T. M. Schutzius, I. S. Bayer, G. M. Jursich, A. Das, and C. M. Megaridis, "Superhydrophobic-superhydrophilic binary micropatterns by localized thermal treatment of polyhedral oligomeric silsesquioxane (POSS)-silica films," *Nanoscale*, vol. 4, pp. 5378–5385, 2012.

[83] K. Tadanaga, J. Morinaga, A. Matsuda, and T. Minami, "Superhydrophobic-superhydrophilic micropatterning on flowerlike alumina coating film by the sol-gel method," *Chemistry of Materials*, vol. 12, no. 3, pp. 590–592, 2000.

[84] X. Zhang, H. Kono, Z. Liu, S. Nishimoto, D. A. Tryk, T. Murakami, H. Sakai, M. Abe, and A. Fujishima, "A transparent and photo-patternable superhydrophobic film," *Chem. Commun.*, pp. 4949–4951, 2007.

[85] J. Huang, Y. Lai, L. Wang, S. Li, M. Ge, K. Zhang, H. Fuchs, and L. Chi, "Controllable wettability and adhesion on bioinspired multifunctional $TiO_2$ nanostructure surfaces for liquid manipulation," *J. Mater. Chem. A*, vol. 2, pp. 18531–18538, 2014.

[86] G. Soliveri, R. Annunziata, S. Ardizzone, G. Cappelletti, and D. Meroni, "Multiscale rough titania films with patterned hydrophobic/oleophobic features," *The Journal of Physical Chemistry C*, vol. 116, no. 50, pp. 26405–26413, 2012.

[87] K. Nakata, S. Nishimoto, Y. Yuda, T. Ochiai, T. Murakami, and A. Fujishima, "Rewritable superhydrophilic-superhydrophobic patterns on a sintered titanium dioxide substrate," *Langmuir*, vol. 26, no. 14, pp. 11628–11630, 2010. PMID: 20552954.

[88] S. Nishimoto, M. Becchaku, Y. Kameshima, Y. Shirosaki, S. Hayakawa, A. Osaka, and M. Miyake, "$TiO_2$-based superhydrophobic–superhydrophilic pattern with an extremely high wettability contrast," *Thin Solid Films*, vol. 558, pp. 221–226, 2014.

[89] H. Hillborg, N. Tomczak, A. Olah, H. Schonherr, and G. J. Vancso, "Nanoscale hydrophobic recovery:? a chemical force microscopy study of UV/ozone-treated cross-linked poly(dimethylsiloxane)," *Langmuir*, vol. 20, no. 3, pp. 785–794, 2004. PMID: 15773106.

[90] Y. Li, Z. Wang, L. M. L. Ou, and H.-Z. Yu, "DNA detection on plastic:? surface activation protocol to convert polycarbonate substrates to biochip platforms," *Analytical Chemistry*, vol. 79, no. 2, pp. 426–433, 2007. PMID: 17222004.

[91] P. M. van Midwoud, A. Janse, M. T. Merema, G. M. M. Groothuis, and E. Verpoorte, "Comparison of biocompatibility and adsorption properties of

different plastics for advanced microfluidic cell and tissue culture models," *Analytical Chemistry*, vol. 84, no. 9, pp. 3938–3944, 2012. PMID: 22444457.

[92] H. Budunoglu, A. Yildirim, M. O. Guler, and M. Bayindir, "Highly transparent, flexible, and thermally stable superhydrophobic ormosil aerogel thin films," *ACS Applied Materials & Interfaces*, vol. 3, no. 2, pp. 539–545, 2011. PMID: 21226471.

[93] H.-C. Kim, C. R. Kreller, K. A. Tran, V. Sisodiya, S. Angelos, G. Wallraff, S. Swanson, and R. D. Miller, "Nanoporous thin films with hydrophilicity-contrasted patterns," *Chemistry of Materials*, vol. 16, no. 22, pp. 4267–4272, 2004.

[94] K. Efimenko, W. E. Wallace, and J. Genzer, "Surface modification of Sylgard-184 poly(dimethyl siloxane) networks by ultraviolet and ultraviolet/ozone treatment," *Journal of Colloid and Interface Science*, vol. 254, no. 2, pp. 306–315, 2002.

[95] H. Budunoglu, A. Yildirim, and M. Bayindir, "Flexible and mechanically stable antireflective coatings from nanoporous organically modified silica colloids," *J. Mater. Chem.*, vol. 22, pp. 9671–9677, 2012.

[96] W.-D. Liu and B. Yang, "Patterned surfaces for biological applications: A new platform using two-dimensional structures as biomaterials," *Chinese Chemical Letters*, vol. 28, no. 4, pp. 675–690, 2017.

[97] Y. Zhang, T. Ren, T. Li, J. He, and D. Fang, "Paper-based hydrophobic/lipophobic surface for sensing applications involving aggressive liquids," *Advanced Materials Interfaces*, vol. 3, no. 22, p. 1600672, 2016.

[98] S. Yang, X. Dai, B. B. Stogin, and T.-S. Wong, "Ultrasensitive surface-enhanced raman scattering detection in common fluids," *Proceedings of the National Academy of Sciences*, vol. 113, no. 2, pp. 268–273, 2016.

[99] L.-P. Xu, Y. Chen, G. Yang, W. Shi, B. Dai, G. Li, Y. Cao, Y. Wen, X. Zhang, and S. Wang, "Ultratrace DNA detection based on the condensing-enrichment effect of superwettable microchips," *Advanced Materials*, vol. 27, no. 43, pp. 6878–6884, 2015.

[100] T. Xu, W. Shi, J. Huang, Y. Song, F. Zhang, L.-P. Xu, X. Zhang, and S. Wang, "Superwettable microchips as a platform toward microgravity biosensing," *ACS Nano*, vol. 11, no. 1, pp. 621–626, 2017. PMID: 27992718.

[101] K. Fukada, N. Kawamura, and S. Shiratori, "Trace material capture by controlled liquid droplets on a superhydrophobic/hydrophilic surface," *Analytical Chemistry*, vol. 89, no. 19, pp. 10391–10396, 2017. PMID: 28872848.

[102] T. Wu, T. Xu, Y. Chen, Y. Yang, L.-P. Xu, X. Zhang, and S. Wang, "Renewable superwettable biochip for miRNA detection," *Sensors and Actuators B: Chemical*, vol. 258, pp. 715–721, 2018.

[103] Y. Chen, L.-P. Xu, J. Meng, S. Deng, L. Ma, S. Zhang, X. Zhang, and S. Wang, "Superwettable microchips with improved spot homogeneity toward sensitive biosensing," *Biosensors and Bioelectronics*, vol. 102, pp. 418–424, 2018.

[104] P. Beyazkilic, U. Tuvshindorj, A. Yildirim, C. Elbuken, and M. Bayindir, "Robust superhydrophilic patterning of superhydrophobic ormosil surfaces for high-throughput on-chip screening applications," *RSC Adv.*, vol. 6, pp. 80049–80054, 2016.

[105] R. Hernandez-Perez, Z. H. Fan, and J. L. Garcia-Cordero, "Evaporation-driven bioassays in suspended droplets," *Analytical Chemistry*, vol. 88, no. 14, pp. 7312–7317, 2016. PMID: 27331825.

[106] Y. Liu, J. Zhu, Y. Xu, Y. Qin, and D. Jiang, "Boronic acid functionalized Aza-Bodipy (azaBDPBA) based fluorescence optodes for the analysis of glucose in whole blood," *ACS Applied Materials & Interfaces*, vol. 7, no. 21, pp. 11141–11145, 2015. PMID: 25962342.

[107] S. Chen, X. Hai, X.-W. Chen, and J.-H. Wang, "In-situ growth of silver nanoparticles on graphene quantum dots for ultrasensitive colorimetric detection of $H_2O_2$ and glucose," *Analytical Chemistry*, vol. 86, no. 13, pp. 6689–6694, 2014. PMID: 24862345.

[108] Z. Mao, Z. Qing, T. Qing, F. Xu, L. Wen, X. He, D. He, H. Shi, and K. Wang, "Poly(thymine)-templated copper nanoparticles as a fluorescent indicator for hydrogen peroxide and oxidase-based biosensing," *Analytical Chemistry*, vol. 87, no. 14, pp. 7454–7460, 2015. PMID: 26112746.

[109] F. He, F. Feng, S. Wang, Y. Li, and D. Zhu, "Fluorescence ratiometric assays of hydrogen peroxide and glucose in serum using conjugated polyelectrolytes," *J. Mater. Chem.*, vol. 17, pp. 3702–3707, 2007.

[110] F. He, Y. Tang, M. Yu, S. Wang, Y. Li, and D. Zhu, "Fluorescence-amplifying detection of hydrogen peroxide with cationic conjugated polymers, and its application to glucose sensing," *Advanced Functional Materials*, vol. 16, no. 1, pp. 91–94.

[111] X. Shen, Y. Shi, B. Peng, K. Li, J. Xiang, G. Zhang, Z. Liu, Y. Chen, and D. Zhang, "Fluorescent polymeric micelles with tetraphenylethylene moieties and their application for the selective detection of glucose," *Macromolecular Bioscience*, vol. 12, no. 11, pp. 1583–1590.

[112] Y. Liu, K. Ai, and L. Lu, "Polydopamine and its derivative materials: Synthesis and promising applications in energy, environmental, and biomedical fields," *Chemical Reviews*, vol. 114, no. 9, pp. 5057–5115, 2014. PMID: 24517847.

[113] A. Yildirim and M. Bayindir, "Turn-on fluorescent dopamine sensing based on in situ formation of visible light emitting polydopamine nanoparticles," *Analytical Chemistry*, vol. 86, no. 11, pp. 5508–5512, 2014. PMID: 24803112.

[114] B. Xiong, Y. Chen, Y. Shu, B. Shen, H. N. Chan, Y. Chen, J. Zhou, and H. Wu, "Highly emissive and biocompatible dopamine-derived oligomers as fluorescent probes for chemical detection and targeted bioimaging," *Chem. Commun.*, vol. 50, pp. 13578–13580, 2014.

[115] S. Quignard, M. d'Ischia, Y. Chen, and J. Fattaccioli, "Ultraviolet-induced fluorescence of polydopamine-coated emulsion droplets," *ChemPlusChem*, vol. 79, no. 9, pp. 1254–1257.

[116] S. Hong, Y. S. Na, S. Choi, I. T. Song, W. Y. Kim, and H. Lee, "Non-covalent self-assembly and covalent polymerization co-contribute to polydopamine formation," *Advanced Functional Materials*, vol. 22, no. 22, pp. 4711–4717, 2012.

[117] X. Yu, H. Fan, Y. Liu, Z. Shi, and Z. Jin, "Characterization of carbonized polydopamine nanoparticles suggests ordered supramolecular structure of polydopamine," *Langmuir*, vol. 30, no. 19, pp. 5497–5505, 2014. PMID: 24773501.

[118] X. Zhang, S. Wang, L. Xu, L. Feng, Y. Ji, L. Tao, S. Li, and Y. Wei, "Biocompatible polydopamine fluorescent organic nanoparticles: facile preparation and cell imaging," *Nanoscale*, vol. 4, pp. 5581–5584, 2012.

[119] X. Chen, Y. Yan, M. Mullner, M. P. van Koeverden, K. F. Noi, W. Zhu, and F. Caruso, "Engineering fluorescent poly(dopamine) capsules," *Langmuir*, vol. 30, no. 10, pp. 2921–2925, 2014. PMID: 24597595.

[120] J.-H. Lin, C.-J. Yu, Y.-C. Yang, and W.-L. Tseng, "Formation of fluorescent polydopamine dots from hydroxyl radical-induced degradation of polydopamine nanoparticles," *Phys. Chem. Chem. Phys.*, vol. 17, pp. 15124–15130, 2015.

[121] M. Bruchez, M. Moronne, P. Gin, S. Weiss, and A. P. Alivisatos, "Semiconductor nanocrystals as fluorescent biological labels," *Science*, vol. 281, no. 5385, pp. 2013–2016, 1998.

[122] J. Escorihuela, M. J. Banuls, R. Puchades, and A. Maquieira, "DNA microarrays on silicon surfaces through thiol-ene chemistry," *Chem. Commun.*, vol. 48, pp. 2116–2118, 2012.